QATAR UNIVERSITY

COLLEGE OF ENGINEERING

CIRCULATING CURRENT MITIGATION AMONG SOURCES IN DC MICROGRID USING DISTRIBUTED SECONDARY CONTROLLERS

BY

AYMAN KHALFALLA

A Thesis Submitted to

the College of Engineering

in Partial Fulfillment of the Requirements for the Degree of

Master of Science in Electrical Engineering

January 2025

COMMITTEE PAGE

The members of the Committee approve the Thesis of
Ayman Khalfalla defended on 01/12/2024.

Prof. Atif Iqbal, *Fellow IEEE*
Thesis/Dissertation Supervisor

Prof. Lazhar Ben-Brahim
Committee Member

Prof. Rashid Alammari
Committee Member

Prof. Ahmed Abu-Siada
Committee Member

Dr. MD Anwarul Hasan
Committee Member

Approved:

College of Engineering

ABSTRACT

Khalfalla, Ayman, H., Masters : January : 2025, Masters of Science in Electrical Engineering

Title: Circulating Current Mitigation Among Sources in DC Microgrid Using Distributed Secondary Controllers

Supervisor of Thesis: Prof. Atif Iqbal, *Fellow IEEE*

Co-Supervisor of Thesis:

In the islanded mode of operation of a DC microgrid, the main objective is to achieve proportional sharing of load power among sources and to maintain the source voltage within the specified limit. The droop control technique is widely used to achieve these objectives. Nevertheless, the performance of the traditional droop control technique becomes poor in the case of DC Microgrid including sources having unequal nominal voltages. The difference in nominal voltages arises due to errors in the measurement of the voltage feedback signal. The unequal values of nominal voltages lead to errors in the proportional sharing of the load current among the source converters. The mismatch in nominal voltages leads to a flow of circulating current among sources. To minimize this circulating current flowing among the sources, various distributed secondary controllers are suggested in the literature. However, these controllers require prior information of circulating current flowing among sources or accurate measurement of line parameters. To resolve these issues, a distributed secondary controller is proposed in this thesis. The proposed controller mainly requires the evaluation of proportional current in order to ensure circulating current minimization. The proportional value of current for a given source is calculated using the formation of power ratings of sources and initial values of its droop gain parameters. The proposed controller ensures the accurate sharing of the load current among source converters in case of a microgrid having sources of unequal capacity or communication link failure. Further, the voltage regulation is maintained within the

defined limit. A small signal model is derived to show the effect of the variation of parameters of the proposed controller on the stability of the DC microgrid. The efficacy of the proposed controller is validated with the help of results capture using the Controller Hardware-in-Loop (CHIL) approach which includes a Real-Time Digital Simulator (RTDS) and Digital Signal Processor (DSP).

DEDICATION

To my parents and siblings,

whose endless support and guidance have been my strength and inspiration.

ACKNOWLEDGMENTS

I want to express my profound gratitude to my supervisor, Prof. Atif Iqbal, *Fellow IEEE*, for his constant support, and wise counsel. His advice has significantly influenced the direction of my research, and I appreciate him sharing his knowledge and experience with me. I sincerely appreciate his hard work and devotion to my accomplishments.

This thesis was made possible by NPRP grant # [13S-0108-200028] from the Qatar National Research Fund (a member of Qatar Foundation). The statements made herein are solely the responsibility of the author.

TABLE OF CONTENTS

LIST OF TABLES

LIST OF FIGURES

CHAPTER 1: INTRODUCTION

1.1 Background

The increase in world energy consumption, the fear of climate change caused by CO_2 emissions, and the diminishing non-renewable resources, encouraged the use of renewable resources. However, to harness energy from these renewable energy sources, a microgrid is considered to be the most appropriate solution. Depending upon the nature of the voltage output, AC and DC microgrids can be used to integrate renewable energy sources. Yet, with the increased loads being DC in nature, renewable sources would require multiple AC-DC and DC-AC conversions resulting in decreased efficiency due to these extra conversions in the case of AC microgrid. To resolve this issue, the use of a DC microgrid is suggested, as it offers an adaptble, flexible, and resilient solution to these modern challenges [1], [2]. Renewable energy sources like solar photovoltaic (PV) sources, fuel cells, and battery storage devices can be directly connected to the DC microgrid. A DC microgrid eliminates the need for source synchronization and power quality problems like harmonics [3]. The DC microgrid's effective efficiency is further enhanced by the lack of skin and proximity effects. [4]. Due to these advantages, the DC microgrid is much preferred over AC microgrid. The concept of the DC microgrid is gaining popularity due to its application in remote electrification to provide power to sensitive loads like military loads, hospitals, and data centres. DC microgrids find their use in potential applications like data centres, electric vehicles, marine vessel charging, telecom stations, etc. [5], [6].

1.2 Thesis Objectives

The difference in nominal voltages arises due to errors in the measurement of the voltage feedback signal. The unequal values of nominal voltages lead to errors in the

proportional sharing of the load current among the source converters. The mismatch in nominal voltages leads to a flow of circulating current among sources.

To overcome the above-mentioned limitations and challenges, a distributed secondary controller is proposed in this thesis to be integrated into the Droop Control system.

This can be achieved through the following objectives:

1. To minimize the circulating current, the proposed secondary controller shifts the droop characteristic parallel to the voltage axis.
2. Investigate existing decentralized control techniques and simulate the proposed control technique.
3. Achieve fair power sharing among various sources in a DC microgrid while ensuring low-voltage regulation for sensitive loads.
4. Implement the control technique in a real-time platform such as RTDS and conduct a comparative study.

1.3 Thesis Contribution

- A new approach to droop controllers in microgrid control has been introduced to ensure balanced power sharing between sources for different loads.
- Traditional droop controllers face power imbalances due to variations in line impedances.
- The new method addresses these imbalances by adjusting the droop gain.
- The approach provides more flexibility and resolves issues like the winding-up problem associated with proportional-integral control.

- A secondary controller enhances performance by sharing current information among sources through a low-bandwidth communication system.
- This enables real-time adaptation of droop characteristics, improving power distribution.

1.4 Thesis Outline

This thesis is structured in five chapters. Chapter 1 provides the background of the study. Chapter 2 presents a comprehensive literature review, along with the methodology employed in this work. The system design is discussed in Chapter 3, detailing the development and configuration of the proposed solution. Chapter 4 covers the simulation and results, providing analysis of the outcomes. Finally, this thesis is concluded in Chapter 5

CHAPTER 2: LITERATURE REVIEW

2.1 Introduction

In a DC Microgrid, energy sources, loads, and storage devices are typically operating on dc voltage. To connect these elements, dc-dc converters are to be used. In an islanded DC Microgrid, renewable resources, and storage components are used for providing energy to the loads as shown in Figure 2.1.

2.2 Role of Converters in DC Microgrids

Source-side converters are used for connecting renewable resources to the dc-bus of the DC microgrid. The storage-side converters (SSCs) are used to connect the battery devices to the loads. Renewable side converters (RSCs) are used to extract the maximum power from renewable resources like photovoltaic (PV) sources and wind turbines and provide it to the storage elements and loads.

2.2.1 Voltage Regulation and Parallel Converter Operation

The purpose of SSC is to regulate the dc-bus voltage at the nominal value. A combination of many dc-dc converters in parallel is preferred over the usage of just a single converter as it ensures more reliability. The malfunctioning converter can be isolated and replaced without disrupting the system as mentioned in [7]. It is easier to add more converters with increased demand by adding more parallel units, while the manufacturing cost and design efforts are reduced [8],[9].

2.3. Control Techniques for Parallel SSCs

The primary objective of parallel operation of SSCs is to ensure fair distribution of the load current among the parallel-connected battery sources while also maintaining

the output voltage across the SSC's output terminals within the acceptable range for the load. The techniques used to achieve these objectives are classified as techniques (i) requiring communication and (ii) techniques that don’t require communication links.

2.3.1 Communication-Based Control Techniques

The Master-Slave control approach is a prominent communication-based method. In this technique, one of the converters operates in voltage-controlled mode (VCM), which is referred to as the Master that regulates the output voltage of the battery source equal to its nominal value. The other converters would operate in current-controlled mode (CCM), referred to as Slave and regulate output current [10]. The controller of the Master converter is responsible for regulating the voltage and providing the necessary current in case of a sudden change in load by taking the difference between the total current provided by slaves and the current demanded by the loads [11]. In this technique, a centralized controller and communication way are required among the converters to operate the system efficiently. As mentioned, this method can be expensive, complex, and low on reliability.

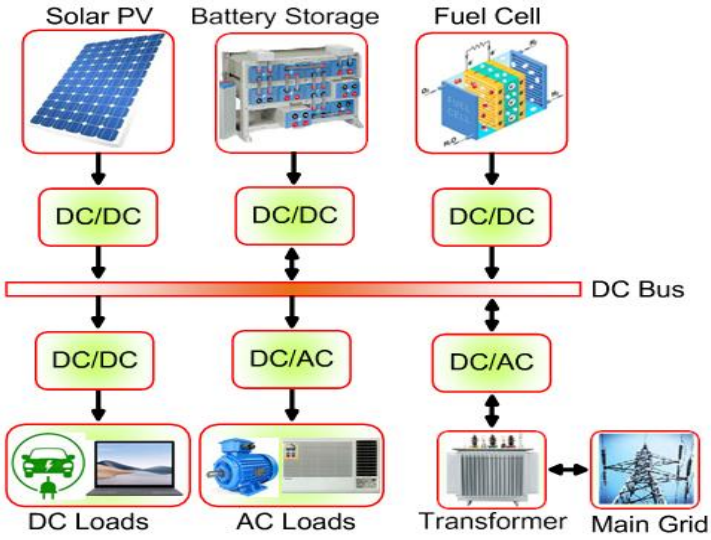

Figure 1. Block diagram of Dc microgrid including sources, loads, and battery storage.

Many papers are reported to resolve issues related to this technique [12], [13]. Nevertheless, this method may introduce high amounts of noise into the system, and an increase in the cost of the overall system. It is typically used in low-power systems.

2.3.2 Techniques Without Communication

To overcome the above-mentioned issues associated with techniques requiring communication, the droop control technique is widely used [14]. In this technique, parallel converters work in voltage control mode and a reference voltage is produced for each converter by the measurement of its parameters which eliminates the need for communication channels among SSC. Using this technique, the system will continue to work without interruptions in case of a communication failure. This increases the reliability of the system. This technique is highly scalable, and each battery source becomes a plug-and-play unit after its connection to the DC Microgrid [15].

2.4 Challenges in Droop Control

Nevertheless, the performance of the traditional droop control technique becomes poor in the case of DC Microgrid including sources having unequal values of nominal voltages. The difference in nominal voltages arises due to errors in the measurement of the voltage feedback signal.

2.4.1 Circulating Current

The unequal values of nominal voltages lead to errors in the proportional sharing of the load current among the source converters. The mismatch in nominal voltages leads to a flow of circulating current among sources. This current produces losses and reduces the efficiency of the DC Microgrid [17]. This current further reduces the useful life of the battery source due to the unnecessary cycling of the battery [16]. The flow of circulating current also leads to the overloading of some of the source converters and may cause premature failure of the power semiconductor devices connected to the source converter [18] [19].

2.5 Circulating Current Mitigation

To resolve this issue, additional controllers are required besides the droop controller. The additional controllers suggested in the literature to minimize circulating current are classified into two broad categories which are (1) controllers requiring no communication (2) controllers requiring communication channels among sources. Controllers requiring no communication and communication links among sources to minimize circulating currents are suggested in [20] and [21].

Table 1: Comparison of the proposed secondary controller with the state-of-the-art secondary controllers suggested in the literature.

S. No.	[R]	Communication type		Current Minimization Performance	Dynamic response	Applicability to microgrid
		All-to-all	Reduced			
1.	[14]	√	x	High	Fast	No
2.	[16]	x	√	High	Slow	Yes
3.	[17]	√	x	High	Fast	No
4.	[20]	x	x	Low	Fast	No
5.	[21]	x	x	Low	Fast	Yes
6.	[24]	√	x	High	Fast	Yes
7.	[25]	x	x	High	Fast	No
8.	[26]	x	x	High	Fast	Yes
9.	[27]	x	x	High	Fast	No
10.	[28]	x	√	High	Slow	Yes
11.	[29]	x	√	High	Slow	Yes
12.	[P]	√	x	High	Fast	Yes

A method based on virtual impedance is proposed [20], whereby the sources' droop gain is adjusted so that the source voltage drop falls within an acceptable range.. However, the suggested method includes the estimation of line resistances which uses additional current sensors and increases the cost of the system. A back-stepping method-based controller is suggested in [21] to minimize the circulating current. The suggested controller minimizes the circulating current among sources by modifying the nominal values of source voltages and maintains the source voltage within the defined limits.

However, the suggested controller is nonlinear and suffers from the limitation of practical applicability. Due to the absence of a communication channel, the proportional current sharing among sources in [20] and [21] may not be very accurate.

To overcome this problem, all-to-all communication-based secondary controllers, are suggested in the literature. Secondary controllers are used to adjust the parameters of droop controllers and minimize the difference in proportional current sharing created due to droop controllers [22]. These controllers require communication among the sources for their implementation. The secondary controllers are used to minimize circulating currents among Sources may be further classified as the controllers including (i) Shift in droop characteristics; and (ii) Modification in droop gain.

Secondary controllers including the shift in droop characteristics of sources are discussed in [14] [16] and [28]. The secondary controller suggested in [14] shifts droop characteristics in the upward direction of the source for which the circulating current is negative. However, in order to evaluate the circulating current, the proposed controller mandates that the DC microgrid must operate at no-load condition only. This option may not be feasible in a DC microgrid having multiple sources and loads. The secondary controller suggested in [14] requires all-to-all communication among sources which may lead to data congestion. To reduce the communication burden, a reduced communication-based secondary controller is suggested in [16] and [28], which modifies the estimation of the average source voltage. However, the reduced communication-based secondary controllers take more time to reach a consensus among the sources and the dynamic response of the system becomes slower [23].

The secondary controller including modification in droop gain of sources is discussed in [17] [24] and [29]. The controller discussed in [17] includes the formulation of an optimization problem, which is used to evaluate optimum values of initial values

of droop gains of the sources. During the operation of the DC Microgrid, droop gains are adjusted adaptively to minimize circulating current flowing between the sources. However, the complexity of the secondary controller increases for a DC microgrid having multiple sources and loads. In [24] and [29], the droop gain of the source is modified to minimize the circulating current flowing among the sources in the DC Microgrid. For this, the line resistance is measured and droop gain is adjusted to make the equivalent output resistance of each source to be identical. However, the suggested techniques used to modify the droop gain are applicable to the radial configuration of the DC microgrid. The performance of the suggested secondary controllers may deteriorate in the case of mesh configuration of the DC microgrid. The techniques discussed in [25] to suppress the circulating current require the accurate measurement of line parameters. The technique suggested in [26] to estimate the line resistance to adjust the droop gain to minimize circulating current is only applicable to the radial configuration of the DC microgrid. The Steepest Decent Method (DSM) which is an optimization-based technique is suggested [27]. The proposed technique adjusts the voltage reference of individual sources in a way to minimize circulating current. However, the practical applicability of the suggested technique is difficult.

Additional challenges associated with distributed secondary controller is ensuring proportional sharing of the load current among sources in case of DC microgrid having sources of unequal capacity. Due to this, some sources may be underloaded and some sources may be overloaded which may lead to premature failure of the converters. The performance of the distributed secondary controllers can also be affected by the delay in the communication links established among sources for information exchange. To enhance the resiliency of the DC microgrid against communication link failure, provision should be there to detect the communication link failure or source failure to

ensure the fail-safe behaviour of the DC microgrid in case of communication link failure [22].

To overcome the above-mentioned limitations and challenges, a distributed secondary controller is proposed in this thesis. The comparison of the proposed controller concerning the state-of-the-art controllers suggested in the literature is listed in Table 1. The salient features of the proposed controller are as follows:

1. To minimize the circulating current, the proposed secondary controller shifts the droop characteristic parallel to the voltage axis.
2. The controller ensures that circulating current is kept to a minimum for all DC Microgrid configurations whether they are radial, mesh, or generic.
3. The controller requires the information of source currents which leads to a reduction in communication data congestion and requires low bandwidth communication.
4. The proposed controller ensures the proportional sharing of load current in case of DC microgrid having sources of unequal capacity. Further, the proposed controller is applicable to radial, mesh or generic configurations of dc microgrid.
5. The proposed controller that the DC microgrid will operate safely even at the event of communication link failure.
6. The proposed controller does not need line resistance data in order to determine the voltage shift.
7. Applicability of the controller is validated for a ring configuration of a DC microgrid having multiple sources and loads.

2.6 Methodology

To achieve proportional sharing of the load current among the source converter with high accuracy, the distributed secondary controller including voltage shift is

proposed. In this section, the procedure for the implementation of the proposed controller is explained.

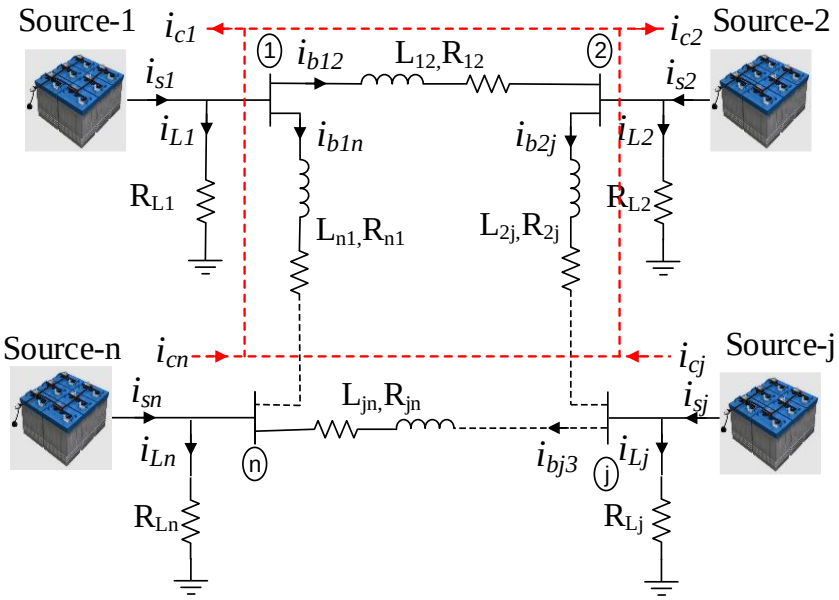

Figure 2. Generalized mesh network of dc microgrid with multiple sources and loads including path of circulating current flowing among sources.

2.6.1 Cause of Circulating Current

Due to errors in the sensors used to sense the output voltage, the nominal voltages of the sources are not equal. The output of these sensors is used as a feedback signal for the voltage controller, which leads to discrepancies in the nominal voltages of sources. Due to unequal values of nominal voltages, the circulating current starts flowing among the sources. The sources having higher values of nominal voltages, which is more than the base value of nominal voltage, starts supplying the circulating current. The sources whose nominal voltages are less than the base value of nominal voltage start sinking the circulating current. A generalized DC Microgrid including the interconnection of various sources and local loads connected across source buses is shown in Fig.2. The envelope of the circulating currents flowing in a ring configuration of a DC Microgrid is shown in Fig 2. Here, i_{s1}, i_{s2}, …, i_{sj}, …, i_{sn} are the currents supplied by the source-1, source-2, …, source-

j, …, source-n. The elements, i_{c1}, i_{c2}, …, i_{cj}, …, i_{cn} represent circulating currents contributed by the source-1, source-2, …, source-j, …, source-n and i_{L1}, i_{L2}, …, i_{Lj}, …, i_{Ln} represent load currents drawn by the load-1, load-2, …, load-j, …, load-n. The currents, i_{b12}, i_{b2j}, …, i_{bjn}, …, i_{bn1} represent branch currents flowing in branch-12, branch-2j, …, branch-jn, …, branch-n1 of DC microgrid. The elements, (R_{12},L_{12}), (R_{2j},L_{2j}), …, (R_{jn},L_{jn}), …, (R_{n1},L_{n1}) represent the resistance and inductance of branch branch-12, branch-2j, …, branch-jn, …, branch-n1 of DC microgrid.

The reference voltage, v_n^{ref} generated by the droop control law in case of n^{th} source is given by,

$$v_n^{ref} = V_n^{nom} - d_n i_{sn} \tag{1}$$

where V_n^{nom} is the nominal voltage of n^{th} source when the source current is zero, d_n is the droop gain and i_{sn} is the source current supplied by the n^{th} source. However, the sources are connected to the load with the nonzero value of cable resistance which cannot be neglected as shown in Fig.3 and Fig. 4. In this case, the equivalent impedance of each source is equal to the algebraic sum of droop gain of the source and the cable resistance as shown in Figs. 3 and 4. In this case, the effective droop gain of the source is modified and the reference value, v_n^{ref} generated by the droop controller is given by

$$v_n^{ref} = V_n^{nom} - (d_n + R_{bn}) i_{sn} \tag{2}$$

The source current supplied by the n^{th} source, i_{sn} consists of two components of currents which can be furnished as actual source current, i_{dn} and circulating current, i_{cn}. The circulating current i_{cn} for n^{th} source may be positive or negative depending upon the magnitude of the nominal voltage of the source. If the source voltage, V_n^{nom} is higher than the base voltage, V^{nom}, then i_{cn} will be positive otherwise negative. On the other hand, if $V_n^{nom} < V^{nom}$, then $i_{cn} < 0$.

To make the idea clearer about the signs of circulating currents flowing in a DC microgrid, consider a two-source microgrid as shown in Fig. 3. From this figure, it is noted that the nominal voltage of source-1, V_1^{nom} is more than the nominal voltage, V^{nom} by a factor of ΔV_1^{nom}. Here, Δv_n^{nom} is the difference between the actual, V_1^{nom} and the base value, V^{nom} of nominal voltage. For source-2, V_2^{nom} is assumed to be smaller than the nominal voltage, V^{nom} by a factor of ΔV_2^{nom}. Due to the unequal values of nominal voltages of source-1 and source-2, the circulating current, I_{c1}=-I_{c2} starts flowing between source-1 and source-2. From Fig.3, it is noted that the circulating currents, I_{c1} and I_{c2} flow through the local circuit formed by source-1 and source-2 not through the load and produces only a heating effect which may reduce the efficiency of the DC microgrid.

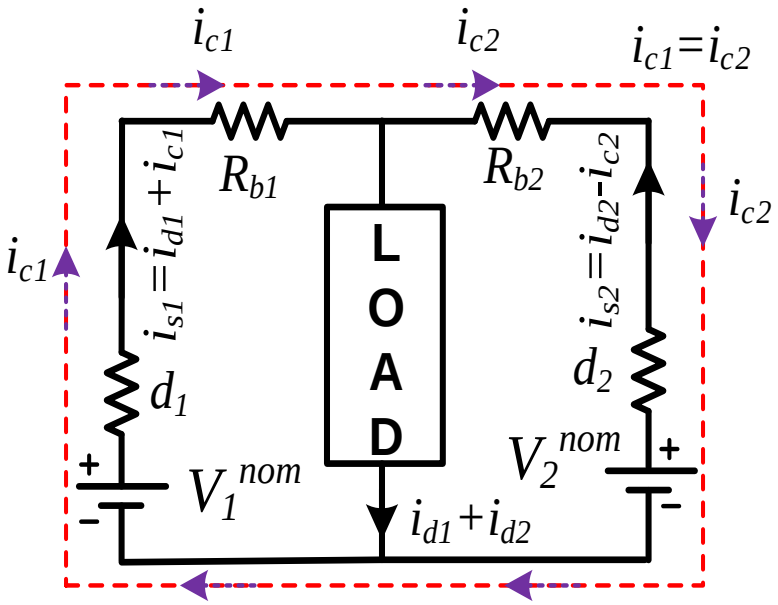

Figure 3. Circulating current flowing in a two-source DC Microgrid.

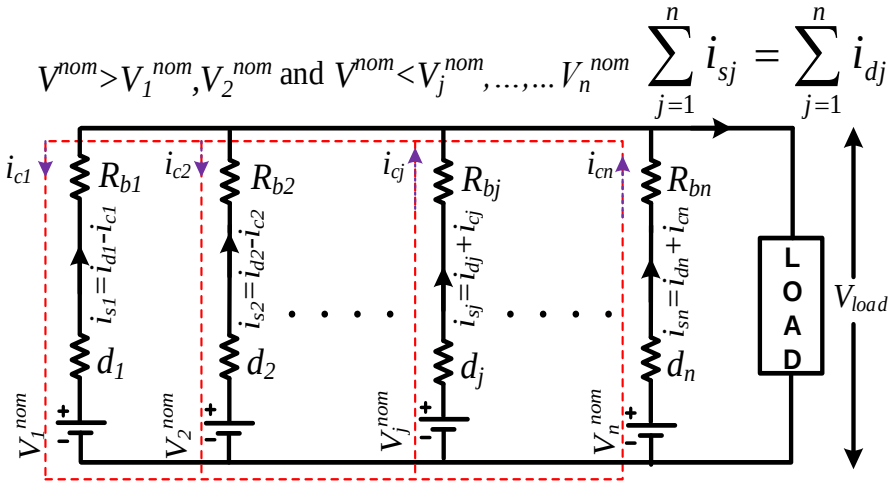

Figure 4. Circulating current flowing in an n-source DC microgrid

Using (1), the reference voltages of source-1 and 2 are

$$\begin{aligned} v_1^{ref} &= V_1^{nom} - d_1 i_{s1} = V_1^{nom} - (d_1 + R_{b1})(i_{d1} + i_{c1}) \\ v_2^{ref} &= V_2^{nom} - d_2 i_{s2} = V_2^{nom} - (d_2 + R_{b2})(i_{d2} - i_{c2}) \end{aligned} \tag{3}$$

where, i_{s1} and i_{s2} represent actual source currents supplied by the source-1 and source-2, i_{d1} and i_{d2} represent the currents supplied by source-1 and souece-2 when nominal voltages of source-1 and source-2 are equal. The elements, i_{c1} and i_{c2} represent the circulating currents contributed by source-1 and source-2. The above explanation is extended for a DC microgrid including n-sources as shown in Fig. 4. From Fig. 4, it is noted that the nominal voltages of source-1 and source-2 are assumed to be less than the nominal voltage, V^{nom} while the nominal voltages of j^{th} source and n^{th} source are assumed to be greater than nominal voltage, V^{nom}. The direction of circulating currents supplied by the respective sources is shown in dotted arrows. The above assumption is made to simplify the analysis which is used to evaluate the circulating currents, i_{c1}, i_{c2}, …, i_{cn} supplied by each source.

For the n^{th} source converter, it is assumed that $V_n^{nom} > V^{nom}$ and Δv_n^{nom} is the difference between V_n^{nom} and V^{nom} which is given by,

$$\Delta V_n^{nom} = V_n^{nom} - V^{nom} \tag{4}$$

For this case, the expression for i_{sn} is

$$i_{sn} = i_{dn} + i_{cn} \tag{5}$$

where i_{dn} represents the components of current supplied by nth source when nominal voltages of all sources are equal. The element, i_{cn} represents the circulating current contributed by source-n. Using (4) and (5), the resultant expression for v_n^{nom} is

$$v_n^{ref} = V^{nom} + \Delta V_n^{nom} - d_n(i_{dn} + i_{cn}) \tag{6}$$

In (6), the effect of cable resistance, R_b is neglected for simplicity. As shown in Fig.4, the values of nominal voltages of source-1, 2 are less than the base value, V^{nom}, while for j^{th} source, V_j^{nom} is greater than V^{nom}. Similar to (6), the expressions for v_1^{ref}, v_2^{ref}, … v_j^{ref} can be derived easily.

From the above discussion, it is observed that the circulating currents, i_{c1}, i_{c2},…, i_{cj},…, i_{cn} start flowing among sources due to unequal nominal voltages, V_1^{nom}, V_2^{nom}, …, V_j^{nom} …, V_n^{nom}. These currents can be minimized by minimizing the voltage offsets, ΔV_1^{nom}, ΔV_2^{nom},…, ΔV_j^{nom} …, ΔV_n^{nom}. However, minimization of these offset voltages requires the measurement of circulating currents, i_{c1}, i_{c2}, …, i_{cj}…, i_{cn} flowing among the source converters which is explained in the next subsection.

2.6.2 Evaluation of circulating currents

In this subsection, the procedure for the evaluation of circulating currents, i_{c1}, i_{c2},…, i_{cn} flowing among the sources is explained.

From the above-mentioned discussion, it is observed that the circulating current is positive for the sources having nominal voltages higher than the base value while their

values are negative for the sources having nominal values of voltages less than the base value. Therefore, the expression for circulating currents supplied by the sources-1, 2, …, n is evaluated using (5) which is given by

$$\begin{aligned} i_{s1} &= i_{d1} - i_{c1} \\ i_{s2} &= i_{d2} - i_{c2} \\ &\vdots \\ i_{sn} &= i_{dn} - i_{cn} \end{aligned} \tag{7}$$

From (7), it is noted that the algebraic sum of source currents will be free from all types of leakage components of currents which can be observed in Fig. 4. As observed from Fig. 4, the circulating currents, i_{c1}, $i_{c2,\ldots,}$ i_{cn} flow through the local circuit formed by the source-1, 2, …, n and not through the load. These currents produce only a heating effect in the DC microgrid. The algebraic sum of source currents leads to the cancellation of all circulating components of currents. Therefore, the average value of current supplied by source-1, 2, …, n is

$$\begin{aligned} i_{avg} &= \frac{i_{s1} + i_{s2} + \ldots\ldots + i_{sn}}{n} = \frac{1}{n}\sum_{j=1}^{n} i_{sj} \\ &= \frac{i_{d1} + i_{d2} + \ldots\ldots + i_{dn}}{n} = \frac{1}{n}\sum_{j=1}^{n} i_{dj} \end{aligned} \tag{8}$$

where n is the total number of sources connected in the DC microgrid. Using (7) and (8), the expression for circulating current supplied by source-1, 2, …, n is approximated as

$$\begin{aligned} i_{c1} &= i_{s1} - i_{avg} \\ i_{c2} &= i_{s2} - i_{avg} \\ &\vdots \\ i_{cn} &= i_{sn} - i_{avg} \end{aligned} \tag{9}$$

The values of circulating currents, i_{c1}, i_{c2},…, i_{cn} supplied by source-1, 2, …, n can be calculated using the expression (9). For the DC microgrid having sources of identical

ratings, the relation $i_{d1}= i_{d2}=...=i_{dn}=i_d$ holds and $i_{avg}=i_{dn}$. From (9), the modified relations for i_{c1}, i_{c2},…, i_{cn} are

$$\begin{aligned} i_{c1} &= i_{s1} - i_d \\ i_{c2} &= i_{s2} - i_d \\ &\vdots \\ i_{cn} &= i_{sn} - i_d \end{aligned} \tag{10}$$

2.6.3 Source with unequal power ratings

The relation given by (10) for evaluating the circulating currents i_{c1}, i_{c2},…, i_{cn} supplied by source-1, 2, …, n is valid for DC microgrid having sources with equal power ratings. However, in practical DC microgrids, the sources with unequal power ratings are usually connected. In this case, the average value of source current, i_{avg} used to calculate the circulating currents will be different for each source. It is because each source contributes to the circulating current according to its power rating. In this case, the systematic procedure to evaluate the average current is discussed.

The droop gain, d for a given source in a DC microgrid is evaluated using the following relation [30]:

$$d = \frac{v_s(V^{nom} - v_s)}{P} \tag{11}$$

where, v_s is the output voltage of the converter when a load of rated power capacity, P is connected across its output. The value of droop gain, d is usually selected in such a way that the voltage regulation across the output terminals is less than 5% of nominal voltage, V^{nom} [22]. If nominal voltages, V_1^{nom}, V_2^{nom},..., V_n^{nom} of all the converters are equal. Therefore, the voltage regulation, V_1^{nom}-v_o for each converter at the rated load will be equal. Using (11), the power ratings, P_1, P_2 ,..., P_n of converters are related to their droop gains, d_1, d_2,..., d_n as follows:

$$P_1 d_1 = P_2 d_2 = ...P_j d_j = ...P_n d_n \tag{12}$$

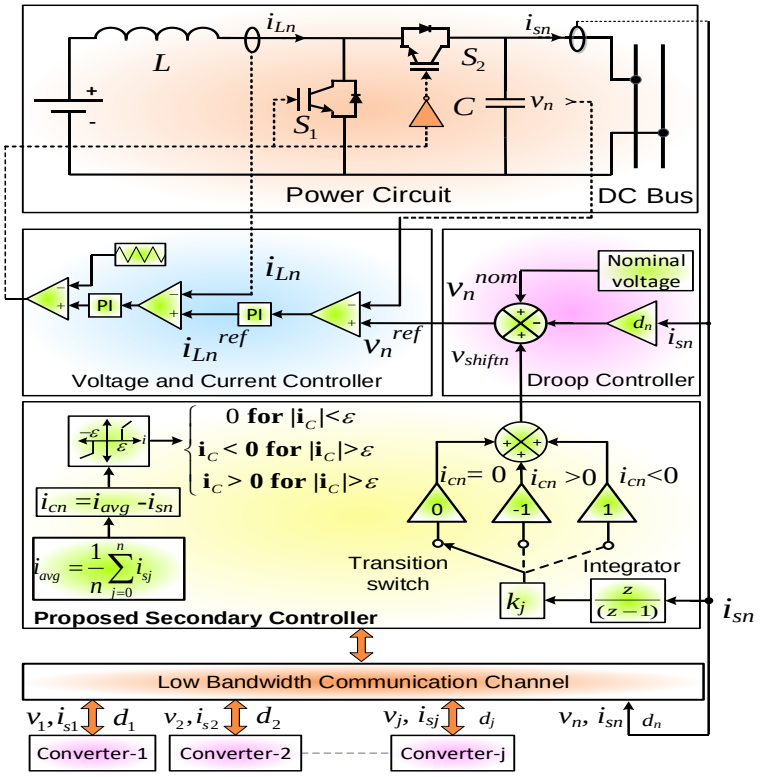

(a)

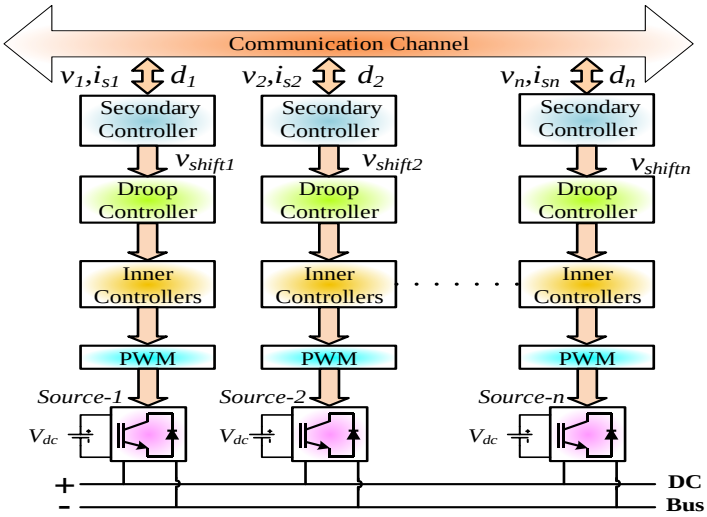

(b)

Figure 5. (a) Control scheme of dc-dc boost converter of nth source with the proposed secondary controller. (b) Distributed nature of proposed secondary controller.

Now considering the case when there is no error in nominal voltages of the source-1, 2, …, n. In this case, the currents, i_{d1}, i_{d2}, ..., i_{dn} supplied by the source-1, 2, …, n are given by

$$i_{d1}d_1 = i_{d2}d_2 = ...i_{dj}d_j = ...i_{dj}d_n \tag{13}$$

Dividing (12) by (13), the resultant expression is

$$\frac{P_1}{i_{d1}} = \frac{P_2}{i_{d2}} ... = \frac{P_j}{i_{dj}} ... = \frac{P_n}{i_{dn}} \tag{14}$$

From (8), the total source current i_s supplied by the source-1, 2 , …, n is

$$\begin{aligned} i_s &= i_{s1} + i_{s2} + ...i_{sj} + ... + i_{sn} \\ &= i_{d1} + i_{d2} + ...i_{dj} + ... + i_{dn} \end{aligned} \tag{15}$$

Substituting the values of i_{d1}, i_{d2}, ..., i_{dj} from (14) in (15), the simplified relation for i_{dn} is

$$i_{dn} = \frac{P_n}{\sum_{i=0}^{n} P_i} \sum_{i=0}^{n} i_{sj} \tag{16}$$

Now the circulating current supplied by the source-n is

$$i_{cn} = i_{sn} - i_{dn} \tag{17}$$

The values of circulating currents, i_{c1}, i_{c2},…, i_{cn} supplied by source-1, 2, …, n can be calculated using the expression (17) in the case of DC microgrid including sources of unequal power ratings.

2.6.4 Minimization of circulating currents

Minimization of circulating currents requires the accurate measurement of circulating currents which are evaluated using the expression (9) and (17). From these expressions, it can be noted that depending upon the values of V_1^{nom}, V_2^{nom}, ..., V_n^{nom}, the

value of circulating currents, i_{c1}, i_{c2}, …, i_{cn} can be either positive or negative. Depending upon the value of i_{cn}, the dead band output, i_{cn} is given by

$$i_{cn} = \begin{cases} 0 \text{ for } |i_{cn}| < \varepsilon \\ i_{cn} < 0 \text{ for } |i_{cn}| > \varepsilon \\ i_{cn} > 0 \text{ for } |i_{cn}| > \varepsilon \end{cases} \tag{18}$$

Depending upon the output of the dead band, the following three cases are possible:

Case-1 ($i_{cn} > 0$)

For, $i_{cn} > 0$, the output of the integrator switches to the left position with the help of the transition switch and the negative voltage shift takes place in droop characteristics of nth source. For this case, the droop characteristics of the n^{th} source are shifted in the downward direction parallel to the voltage axis by the proposed secondary controller. Assuming that the vertical shift in the droop characteristic of n^{th} sources is v_{shiftn} provided by the secondary controller, the output of the droop controller is

$$v_n^{ref} = v_n^{nom} - v_{shiftn} - d_n i_{sn} \tag{19}$$

Case-2 ($i_{cn} < 0$)

For, $i_{cn} < 0$, the output of the integrator switches to the right position with the help of the transition switch and the positive voltage shift takes place in droop characteristics of nth source. For this case, the droop characteristic of n^{th} source is shifted in the upward direction and the modified droop law is given by

$$v_n^{ref} = v_n^{nom} + v_{shiftn} - d_n i_{sn} \tag{20}$$

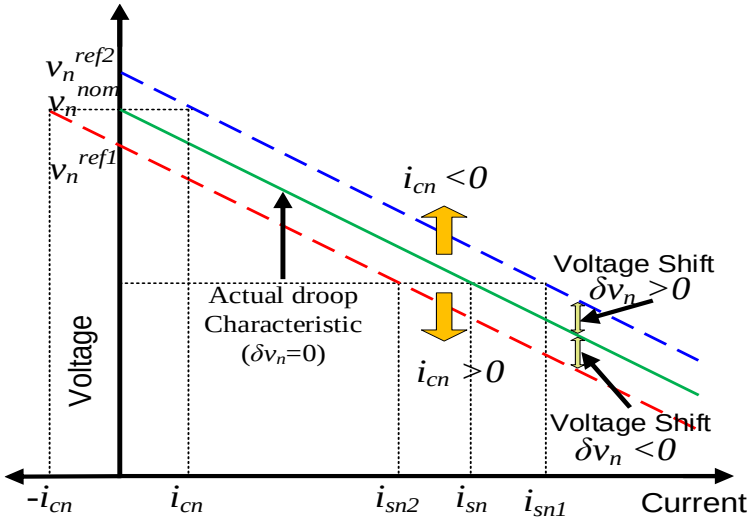

Figure 6. Effect of proposed controller on the droop characteristics of nth

To ensure oscillation-free convergence of the controller about the operating point of the DC microgrid, a tolerance, ε is defined for the circulating current. Therefore, the shift in the droop characteristic of n^{th} source continues until and unless the magnitude of the circulating current becomes less than the tolerance limit, ε.

For the value of $|i_c| > \varepsilon$, the value of v_{shiftn} for n^{th} source is evaluated using the following relation,

$$v_{shiftn}[n] = v_{shiftnt}[n-1] + k_n i_{sn}[n] \tag{21}$$

Here, $v_n[n]$ is the new and $v_n[n\text{-}1]$ is the previous value of the voltage shift, v_{shiftn} respectively. The element, k_n is a constant. It determines the rate of convergence of circulating current, i_{cn} towards ε. By increasing the value of k_n, *fast convergence of* i_{cn} towards ε can be ensured. However, the large value of k_n may lead to an oscillatory response of the DC microgrid about the operating point. DSP is used to execute the equation (21). The time period during which the value of δv_n is updated in a DSP is T_s. Taking z-transformation of (21), the expression for v_{shiftn} is given by

$$v_{shiftn}[n] = \frac{z}{1-z} k_n i_{sn}[n] \tag{22}$$

The relation for v_{shiftn} in the time domain can be written as

$$v_{shiftn}(t) = \frac{k_n}{T_s}\int_0^t i_{sn}(t)dt \tag{23}$$

Taking the derivative of both sides, the first-order differential equation representing the dynamics of the secondary controller is

$$\frac{dv_{shiftn}(t)}{dt} = \frac{k_n}{T_s} i_{sn}(t) \tag{24}$$

Case-3 (i_{cn}=0)

From (18), it is noted that for $|i_{cn}|<\varepsilon$, the output of dead band block will be zero. The integrator included in the proposed secondary will not integrate the input $k_n i_{sj}$ and the voltage shift, v_{shift} will be restored to its previous value, $v_{shift}[n-1]$. Therefore, the n^{th} source continues to share its power as per normal droop control law.

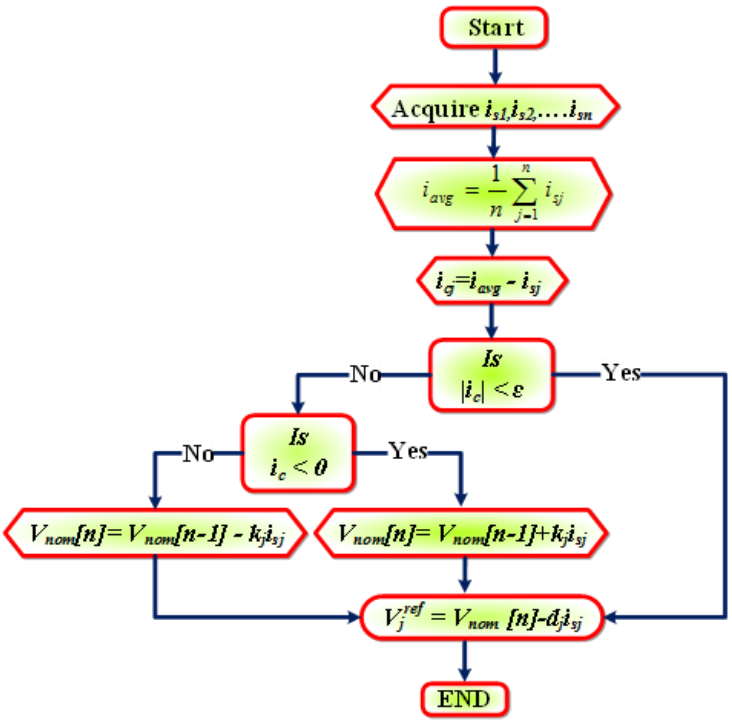

Figure 7. Algorithm of proposed distributed secondary controller to ensure voltage shift in droop characteristics of nth source.

2.6.5 Evaluation of vshiftn

The corrective term of the nth source is evaluated by the secondary controller of the nth source using the relation (21). Assuming that the secondary controller starts its control action at time $t=t_1$. Before the time instant $t=t_1$, the output of the secondary controller will be zero. As soon as the secondary controller is initiated, the initial output of the secondary controller will be $k_n i_{sn}$. If the magnitude of the circulating current, i_{cn} is greater than the tolerance limit, ε, the secondary controller starts the integration of its output until and unless the current i_c is reduced to $|i_{cn}|< \varepsilon$. During this procedure, the reference voltage of nth source given by (19) keeps on increasing which shifts the droop characteristic in the upward direction. To ensure the stable operation of the dc microgrid, the initial value of k is chosen in such a way that $k_n< d_n$. As soon as the circulating current is converged to the condition, $|i_{cn}|< \varepsilon$, the output of the secondary controller is fixed to the last sampled value, $v_{shiftn}\ [n]$ given by (21) and the secondary stops modifying the voltage reference value, v_n^{ref}. Using the updated value of nominal voltage, the reference output voltage is generated which is given by

$$v_n^{ref}[n]=v_n[n]+v_{shiftn}[n]-d_n i_{sn}[n] \tag{25}$$

2.6.6 Evaluation of vshiftn Control Scheme of the Converter

In the case of a DC microgrid, dc-dc boost converters are normally used to interface the battery source to the source bus in the DC microgrid. The dc-dc boost converters step up the battery voltage and reduce the requirement for a greater number of battery sources. The control scheme of the boost converters including the proposed secondary controller used to minimize the circulating current of n^{th} source is shown in Fig. 5(a). The distributed nature of the proposed secondary controller is represented in Fig. 5(b). The droop controller and inner loop controllers (voltage and current

controllers) are shown in Fig. 5(a). First of all, the information corresponding to all source currents is supplied to the n^{th} source using the communication channel. Using this, the average value of the source current is calculated using (8).

Now, the value of circulating current supplied by the n^{th} source is evaluated using (9). If the magnitude of i_{cn} is greater than ε, a shift δv_{shiftn} is provided in the reference value of voltage, v_n^{ref}. Depending upon the sign of i_{cn}, the magnitude δv_{shiftn} can be positive as well as negative. For, $i_{cn} > 0$, the voltage shift, δv_{shiftn} is negative and for $i_{cn} < 0$, the voltage shift, δv_{shiftn} is positive. The effect of voltage shift on the droop characteristics of n^{th} source is shown in Fig. 6.

Fig. 7 shows the flow chart of the proposed secondary controller used to provide voltage shift in droop characteristic of n^{th} source. From this chart, it observed that to execute the desired control task, the information corresponding to source currents, i_{s1}, $i_{s2}, \ldots, i_{sn}$ is acquired using a low bandwidth communication channel among the sources. Using this information, the average values of source current, i_{avg} is calculated using (8). Now using (9), the circulating current supplied by the n^{th} source is evaluated. If the magnitude of the circulating current is greater than the tolerance limit, ε, the proposed secondary controller starts shifting droop characteristics of n^{th} source. Depending upon the sign of i_{cn}, these characteristics may be shifted in the upward or downward direction. For $|i_{cn}| < \varepsilon$, the secondary controller stops modifying the nominal voltage of the source and the magnitude of the voltage shift remains fixed at its previous value.

2.6.7 Use of low bandwidth communication channel

The proposed distributed secondary controller requires the information of the currents, supplied by the source-1, 2 …, n for its implementation. This information can be acquired with the help of a communication channel having low bandwidth like

Controller Area Network (CAN) communication. This leads to a reduction in the cost of the system and makes the proposed scheme to be an economical one.

2.6.8 Fail-safe behaviour of DC microgrid in case of communication link failure.

In the event of a communication link failure, the proposed distributed secondary controller's performance degrades, resulting in an inability to entirely limit circulating currents among the sources. This leads to increased circulating currents, load imbalance, and poor voltage regulation, all of which can have an influence on the overall efficiency and lifespan of the DC microgrid components. Communication delays, even in the absence of a major failure, can have an impact on the system's dynamic reaction, dropping the controller's effectiveness in real-time applications. To address these issues, a fault detection technique, as described in [31] and [32], is used to locate and isolate faulty links or sources. This method ensures that the DC microgrid runs securely by maintaining minimum circulating currents and proportional load sharing even in the presence of such disturbances.

2.7 Summary

The literature study investigates the basic components and control mechanisms utilized in DC microgrids, with an emphasis on circulating currents and voltage management. It illustrates how source-side and storage-side converters work together to keep the DC bus voltage stable while connecting renewable sources and loads. The chapter compares communication-based control systems, such as the Master-Slave approach, with non-communication-based ones, including droop control. While droop control is commonly used because to its scalability and simplicity, it has limitations such as uneven load sharing and a generation of circulating currents. The analysis classifies

secondary controllers into those that require communication and those that do not, and explains how each technique minimizes circulating currents. However, issues such as data congestion, slow dynamic response, and mistakes in current measurement remain prevalent. The suggested distributed secondary controller solves these issues by providing a new method of shifting droop characteristics without the need for complex communication infrastructure. The chapter highlights this research as filling an essential need in ensuring stable, effective, and scalable microgrid operations.

CHAPTER 3: SYSTEM DESIGN

3.1 Introduction

This Chapter explains the modeling of the various elements of the DC microgrid like sources, loads and interconnecting network including the proposed secondary controller. A linearized small signal model of the DC microgrid is derived which is used to study the effect of variation of parameters of the proposed controller on the stability of the DC microgrid. The linearized small signal model is derived for the mesh configuration of the DC microgrid shown in Fig. 2. However, the derived model applies to the radial, ring or generic of the two configurations. As shown in Fig. 5(a), the dc-dc boost converters are used to configure the sources to the buses of the DC microgrid. The dynamics of the inner loop voltage and current controller are assumed to be much faster than the dynamics of the outer droop control loop. Therefore, to study the dynamic response of the DC microgrid including the proposed controller, a reduced order model is used in which the dynamics of inner voltage and the current control loop are neglected without affecting the accuracy of the analysis.

From (1), the reference voltage generated by the droop controller is

$$v_n^{ref}(t) = v_n^{nom} + \delta v_n(t) - d_n i_{sn}(t) \tag{26}$$

Here, v_n^{ref} is taken as v_s which represents the source voltage of n^{th} converter. Linearizing both sides and writing in matrix form for a DC microgrid having multiple sources and loads,

$$\Delta \boldsymbol{v_s}(\boldsymbol{t}) = \Delta \boldsymbol{v_{shift}}(\boldsymbol{t}) - \boldsymbol{D}\Delta \boldsymbol{i_s}(\boldsymbol{t}) \tag{27}$$

where, $\Delta vs(t)$, $\Delta vshift(t)$ and $\Delta i_s(t)$ are the column vectors of deviations in source voltages, voltage shifts in source voltage and source currents, respectively. Here, the element D is a diagonal matrix and the expression is $D= diag[d1, d2, . . . , dn]$.

Now the linearized relation derived for the load and the interconnecting network which is discussed in [33] is included. The voltage across the bus-*i* and bus-*j* of DC microgrid is given by

$$v_i(t) - v_j(t) = L_{ij}\frac{di_{ij}(t)}{dt} + R_{ij}\Delta i_{ij}(t) \tag{28}$$

where R_{ij} and L_{ij} are the resistance and inductance of ij^{th} branch of the DC microgrid. Linearizing (28) and writing in the matrix for the DC microgrid, the linearized column vector of branch voltage, Δv_b is

$$\Delta v_b(t) = \boldsymbol{M}\Delta v_s(t) = \boldsymbol{L_b}\frac{di_b(t)}{dt} + \boldsymbol{R_b}\Delta i_b(t) \tag{29}$$

where, $\Delta v_b(t)$ and $\Delta ib(t)$ are the column vector of branch voltages and branch currents, respectively. Here, $L_b = diag[L_{b1}, L_{b2}, ...L_{bn}]$ and $R_b = diag[R_{b1}, R_{b2}, ...R_{bn}]$ are the diagonal matrices of cable inductances and cable resistances, respectively. M is the incidence matrix of the DC microgrid network. As shown in Fig. 2, resistive loads are assumed to be connected across each source bus. The current, $i_{Lj}(t)$ drawn by the load, R_{Lj} connected at bus-j is

$$v_{sj}(t) = R_{Lj}i_{Lj}(t) \Rightarrow i_{Lj}(t) = G_{Lj}v_{sj}(t) \tag{30}$$

Linearizing (30) and writing in matrix form, the linearized relation for the load current in matrix form is,

$$\triangle \boldsymbol{i}_L(t) = \boldsymbol{G_L} \triangle v_s(t) \tag{31}$$

Applying Kirchoff Current Law (KCL) at source bus-j, the load current, $i_{Lj}(t)$ and source current, $i_{sj}(t)$ and branch current, $i_{ij}(t)$ are related to each other by the following relation:

$$\boldsymbol{i}_{sj}(t) = \boldsymbol{i}_{Lj}(t) + \boldsymbol{i}_i(t) - \boldsymbol{i}_j(t) \tag{32}$$

Applying Kirchoff Current Law (KCL) at each source bus, and linearizing the load current, $\Delta i_L(t)$ and source current, $\Delta i_s(t)$ and branch current, $\Delta i_b(t)$ are related to each other by the linearized relation given by

$$\triangle \boldsymbol{i}_s(t) = \triangle \boldsymbol{i}_L(t) + \boldsymbol{M}^{\boldsymbol{T}} \triangle \boldsymbol{i}_b(t) \tag{33}$$

Substituting the value of $\Delta i_L(t)$ from (31) in (33), the simplified expression of $\Delta i_s(t)$ is

$$\triangle \boldsymbol{i}_s(t) = \boldsymbol{G}_{\boldsymbol{L}} \triangle \boldsymbol{v}_s(t) + \boldsymbol{M}^{\boldsymbol{T}} \triangle \boldsymbol{i}_b(t) \tag{34}$$

Now substituting the value of $\Delta i_s(t)$ from (34) in (27), the simplified relation for Δv_s is

$$\triangle v_s(t) = -(\boldsymbol{I}+\boldsymbol{D}\boldsymbol{G}_{\boldsymbol{L}})^{-1} \triangle v_{shift}(t) - (\boldsymbol{I}+\boldsymbol{D}\boldsymbol{G}_{\boldsymbol{L}})^{-1} \boldsymbol{D}\boldsymbol{M}^{\boldsymbol{T}} \triangle i_b(t) \tag{35}$$

Substituting the value of $\Delta v_s(t)$ in (28), the linearized relation for $\Delta i_b(t)$ is

$$\frac{d\triangle i_b(t)}{dt} = -\boldsymbol{L}_{\boldsymbol{b}}^{-1}\boldsymbol{M}(\boldsymbol{I}+\boldsymbol{D}\boldsymbol{G}_{\boldsymbol{L}})^{-1} \triangle \delta v(t) - \boldsymbol{L}_{\boldsymbol{b}}^{-1}(\boldsymbol{M}(\boldsymbol{I}+\boldsymbol{D}\boldsymbol{G}_{\boldsymbol{L}})^{-1}\boldsymbol{D}\boldsymbol{M}^{\boldsymbol{T}}+\boldsymbol{R}_{\boldsymbol{b}}) \triangle i_b(t) \tag{36}$$

Fig. 5(a) shows the control scheme of the dc-dc boost converter along with the voltage shift-based secondary controller. Relation (22) gives the dynamics of the controller in a discrete domain. From (24), the dynamics of the voltage shift controller is represented using first order differential equation in the time domain as,

$$\frac{dv_{shiftj}(t)}{dt} = \frac{k_{sj}}{T_s} i_s(t) \tag{37}$$

Linearizing (37) and writing in matrix form as,

$$\frac{d\boldsymbol{v}_{shift}(t)}{dt} = \frac{\boldsymbol{K}_{\boldsymbol{s}}}{\boldsymbol{T}_{\boldsymbol{s}}} \triangle \boldsymbol{i}_s(t) \tag{38}$$

Here, $K_s = diag[K_{s1}, K_{s2}, \ldots K_{sn}]$ is the diagonal matrices of coefficients. Substituting the value of $\Delta i_s(t)$ from (24) in (38), the simplified relation for $\Delta v_{shift}(t)$ is,

$$\frac{d\triangle \boldsymbol{v}_{shift}(t)}{dt} = \frac{\boldsymbol{K}_{\boldsymbol{s}}}{\boldsymbol{T}_{\boldsymbol{s}}} [\boldsymbol{G}_{\boldsymbol{L}}] \triangle \boldsymbol{v}_s(t) + \frac{\boldsymbol{G}_{\boldsymbol{s}}}{\boldsymbol{T}_{\boldsymbol{s}}} \boldsymbol{M}^{\boldsymbol{T}} \triangle \boldsymbol{i}_b(t) \tag{39}$$

Substituting the value of $\Delta v_s(t)$ from (35) in (39), the simplified relation for $\Delta v_{shift}(t)$ is

$$\frac{d\triangle v_{shift}(t)}{dt} = -\frac{G_s G_L}{T_s}(I + DG_L)^{-1} \triangle v_{shift}(t) + \frac{G_s}{T_s}[I - G_L(+DG_L)^{-1}D]M^T \triangle i_b(t) \tag{40}$$

The linearized model given by (36) and (40) can be represented in standard state variable form,

$$\dot{\triangle x}(t) = A\Delta x(t) \tag{41}$$

Here, $\Delta x(t)$ is a column vector of state variables and $\Delta x(t) = [\Delta v_{shift}(t)\ \Delta i_b(t)]^T$. The relation (41) is used to study the effect of variation of parameters of the DC microgrid on the stability of the system.

The inner voltage and current control loop dynamics are faster than the droop control and secondary control loop. Therefore, the dynamics of voltage and current control loops are neglected.

3.2 Summary

The system design chapter provides a technical but clear overview of the proposed distributed secondary controller's configuration. It begins by describing the components of a typical DC microgrid, such as the sources, loads, and interconnecting cables. The proposed controller is integrated into a droop-based system, which utilizes voltage shifting to reduce circulating currents while maintaining proportional load sharing. To assess the microgrid's dynamic behavior, a reduced-order model is built, simplifying complex interactions while maintaining the required accuracy. This model focuses on essential elements that affect system stability, such as droop gains, line resistances, and branch currents.

CHAPTER 4: SIMULATION RESULTS

4.1 Introduction

The linearized model given by (41) is derived for a mesh configuration of the DC Microgrid shown in Figure 2. However, it is equally applicable for radial and ring configurations. To simplify the analysis, the DC Microgrid including three sources, and three loads connected across source buses and these sources are connected in the form of ring configuration as shown in Fig. 8 is considered. The parameters of the DC Microgrid are listed in Table 2 while the parameters of the DC interconnecting network are included in Table 3. The switching frequency of the dc-dc boost converter used to interface the battery to the source bus is 5 kHz. Corresponding to this, the parameters of the inner current controller are tuned in such a way that the phase margin of the inner current controller is 86. 63^{o} which is achieved at a crossover frequency of 1 kHz. The phase margin of the voltage controller is 55.82^{o} which is achieved at a crossover frequency of 25 Hz. The initial value of droop gain of each source is 0.0475 Ω. The value of the coefficient, k for each source is set to 100μV/A and the value of tolerance, ε is 0.5% of the rated value of source current.

Table 2: Parameters of DC Microgrid

S. No.	Parameters	Values
1.	Rated Power	100 kW
2.	Nominal value of source voltage	400 V
3.	Load Resistance	1.6 Ω
4.	Series Inductor	2 mH
5.	Parallel Capacitor	3000 μF
6.	Required Voltage Regulation	5%
7.	Error in measurement	1%
8.	Droop Gain	0.0465 Ω
9.	Current controller	0.16 +120/s
10	Voltage controller	0.3 + 80/s

Table 3: Parameters of interconnecting cables

S. No.	Parameters	Branch		
		12	23	31
1.	Cable length	550 m	550 m	550 m
2.	Current rating	250 A		
3.	Cable type	3 conductor Al-PVC 185 mm2		
4.	Resistance	0.152 mΩ/meter		
5.	Inductance	0.237 μH/meter		

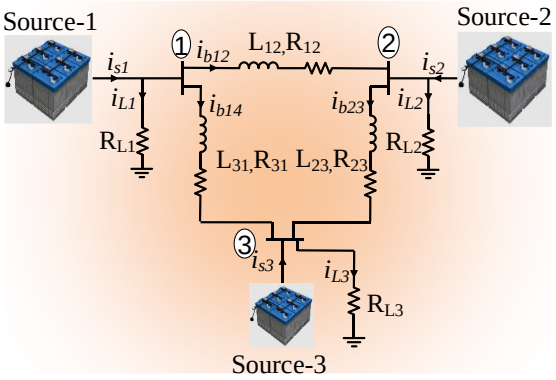

Figure 8. Ring configuration of DC Microgrid including three sources and loads.

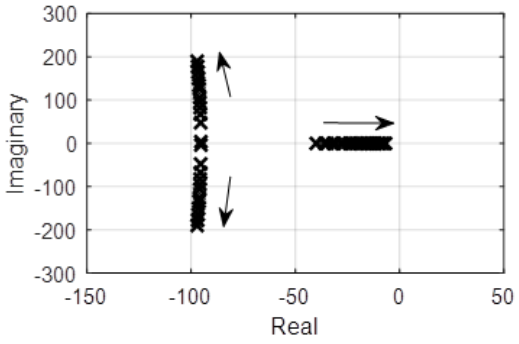

Figure 9. Eigenvalues root loci plot for variation in values of coefficient, kn

4.2 Simulation Results

For the abovementioned parameters of the DC Microgrid, the eigenvalues of the DC Microgrid are plotted in a complex frequency plane. Fig. 9 shows the effect of the increment of coefficient, k_n on the stability of DC Microgrid. From this plot, it is observed that the dominant eigenvalues of the DC Microgrid start shifting towards the Right-Hand Plane (RHP) for increasing values of k_n. Some of the eigenvalues start shifting away from the real axis which indicates the oscillatory operation of dc

microgrid. For high values of coefficient, k, the stability margin of the DC Microgrid decreases, and the operation of the DC Microgrid becomes unstable.

4.3 Performance of the proposed secondary controller with sources having equal power ratings

To study the performance of the proposed secondary including the source having equal power ratings, the ring configuration of the DC microgrid as shown in Fig. 8. is simulated in Matlab/Simulink. The parameters of the microgrid are listed in Table 2. The power rating of each source converter is 100 kW and the droop gain, d of each converter is calculated using (11) and is found to be 0.076Ω for voltage regulation of 5% of the base nominal voltage, 400V. The value of the tolerance limit, ε is set to 0.5% of the rated value of source current. The error in nominal voltages of source-1 and 3 is assumed to be -1% and 1% of the base nominal voltage, Vnom. The initial value of the load connected across bus-1, bus-2 and bus-3 is 50 kW each. Therefore, the initial value of circulating current contributed by the source-1, 2 and 3 are -36A, 14A and 22A. At time instant, t=0.2s, the step variation in load demand from 50kW to 60kW at bus-2 and from 50 kW to 70kW at bus-3 is applied. Due to the increment in load demand, the circulating currents contributed by source-1, source-2 and source-3 are further modified and the resultant values of these currents are -44A, 7A and 37A, respectively. The proposed secondary controller is started at the time instant of t=0.4s. In the case of equal power ratings of sources, the circulating current contributed by various is evaluated using (9). Depending upon the sign of circulating current, ic, the proposed secondary controllers start shifting droop characteristics of source-1 in the upward direction and source-2, 3 in the downward direction as shown in Fig. 10(c). From Fig. 10(a), it is noted that the circulating currents, i_{c1}, i_{c2} and i_{c3} are reduced to the tolerance limit, ε. Fig. 10(b) shows that the initial currents supplied by source-1, 2 and 3 are 183A, 154A and 102A

respectively. Due to the secondary controller action, these currents are converged to the average value of source current, i_{avg}=147A. Waveforms of the voltages across the output of source-1, source-2 and source-3 are shown in Fig. 10(c). The voltage regulation across the output terminal of source-1, 2 and 3 are observed to be 2.5%, 2.5% and 3.25% of the base nominal voltage, 400V.

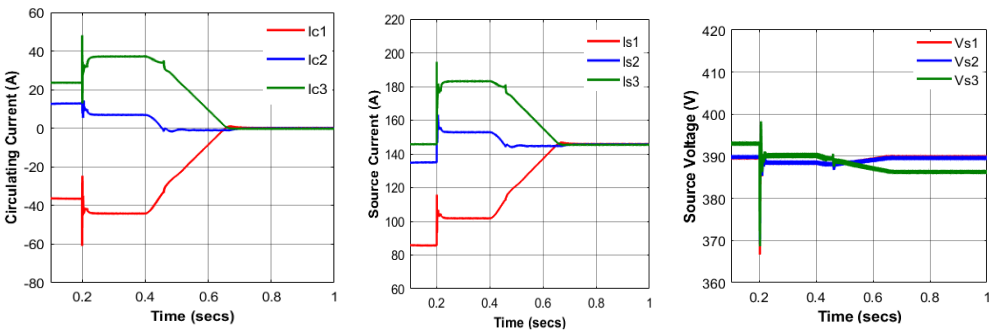

Figure 10. Waveforms of (a) Circulating currents, i_{c1}, i_{c2} and i_{c3} (b) Source currents, i_{s1}, i_{s2} and i_{s3}. (c) Source voltages, v_{s1}, v_{s2} and v_{s3} in case of DC microgrid including sources with equal capacity of 100kW each.

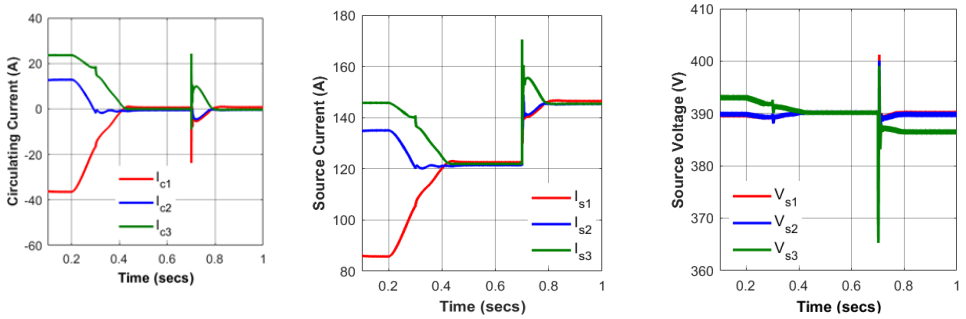

Figure 11. Waveforms of (a) Circulating currents, i_{c1}, i_{c2} and i_{c3} (b) Source currents, i_{s1}, i_{s2} and i_{s3}. (c) Source voltages, v_{s1}, v_{s2} and v_{s3}.

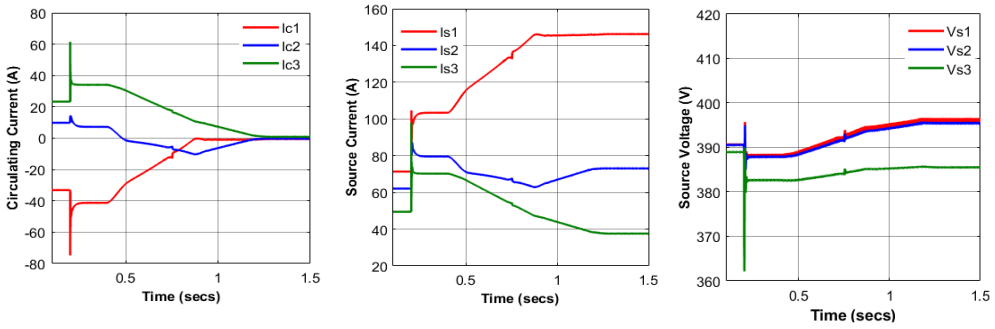

Figure 12. Waveforms of (a) Circulating currents, i_{c1}, i_{c2} and i_{c3} (b) Source currents, i_{s1}, i_{s2} and i_{s3}. (c) Source voltages, v_{s1}, v_{s2} and v_{s3} in case of DC microgrid having sources of unequal ratings. The capacity of Source-1 is 100 kW, source-2 is 50 kW and that of source-3 is 25 kW.

Now the performance of the proposed distributed secondary controller is validated for a condition when the controller is activated and step variation in load demand is applied. The initial values of the loads connected across bus-1, bus-2 and bus-3 are 50 kW each. Therefore, the initial value of circulating current contributed by the source-1, 2 and 3 are -36A, 14A and 22A which can be observed from Fig. 11(a). The proposed secondary controller is switched on at time instant, t=0.2s. Depending upon the sign of circulating current, ic, the proposed secondary controllers

start shifting droop characteristics of source-1 in the upward direction and source-2, 3 in the downward direction as shown in Fig. 11(c). From Fig. 11(a), it is noted that the circulating currents, ic1, ic2 and ic3 are reduced to the tolerance limit, ε. From Fig. 11(b), it is noted that the initial values of currents supplied by source-1, 2 and 3 are 146A, 135A and 86A, respectively. However, due to the controller action initiated at time instant, t=0.2, the currents supplied by source-1, 2 and 3 start converging towards the average value of current to be supplied by each converter which is iavg=123A.

Waveforms of the voltages across the output of source-1, source-2 and source-3 are shown in Fig. 11(c). The voltage regulation across the output terminal of each source is observed to be 2.5% of the base nominal voltage, 400V. At time instant, t=0.7s, the step variation in load demand from 50kW to 60kW at bus-2 and from 50 kW to 70kW at bus-3 is applied. From Fig. 11(a), it is noted that the controller is active and

takes immediately the control action. Due to controller action, the circulating current contributed by each source is reduced to the tolerance limit, ε. The source current supplied by each source is reduced to the average value of 147A as shown in Fig. 11(b). The voltage regulation across the output terminal of source-1, 2 and 3 are observed to be 2.5%, 2.5% and 3.25% of the base nominal voltage, 400V.

4.4 Performance of the proposed secondary controller with sources having unequal power ratings

To validate the performance of the proposed distributed secondary controller, the DC microgrid including three sources having rated power capacity of 100kW, 50kW and 25 kW is considered. The droop gains selected for source-1, 2 and 3 for voltage regulation of 5% of the nominal voltage are 0.076Ω, 0.152Ω and 0.304Ω, respectively. The nominal voltage of source-2 is 400V while errors of -1% and 1% are

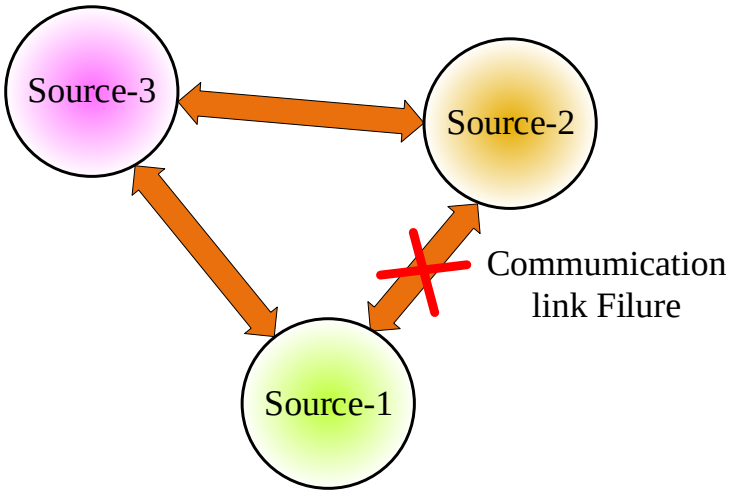

Figure 13. Communication link failure between source-1 and 2.

considered in the nominal voltages of source-1 and source-3, respectively. The initial value of the load connected across bus-1, bus-2 and bus-3 are 25kW each. Therefore, the initial value of circulating current contributed by the source-1, 2 and 3 are -33A, 10A and 23A. At time instant, t=0.2s, the step variation in load demand from 25kW to 35kW at bus-2 and from 25kW to 45kW at bus-3 is applied. Due to the increment in load demand, the circulating currents contributed by source-1, source-2 and source-3 are further modified and the resultant values of these currents are -41A,

7A and 34A, respectively. The proposed secondary controller is started at the time instant of t= 0.4 s. In case of unequal power ratings of sources, the circulating current contributed by various is evaluated using (15). Depending upon the sign of circulating current, i_c, the proposed secondary controller starts shifting droop characteristics either in the upward or downward direction. From Fig. 12(a), it is noted that the circulating currents, i_{c1}, i_{c2} and i_{c3} are reduced to the tolerance limit, ε which is 0.5%. Fig. 12(b) shows that due to the secondary controller action, the currents supplied by source-1, 2 and 3 are reduced to average values of source-1, 2 and source-3 currents which are 150A, 75A and 37.5A respectively. Waveforms of the voltages across the output of source-1, source-2 and

source-3 are shown in Fig. 12(c). The voltage regulation across the output terminal of source-1, 2 and 3 are observed to be 0.75%, 1% and 3.25% of the base nominal voltage, 400V.

4.5 Operation of the proposed secondary controller in the event of a communication link failure

To validate the performance of the proposed secondary controller during link failure, it is assumed that communication link failure occurs between the source-1 and source-2 as shown in Fig. 13. Due to communication failure,

the secondary controller of source-3 will have the information corresponding to the currents supplied by source-1 and source-2. However, the secondary controllers included with source-1 and source-2 will have information of currents supplied by source-1, 3 and source-2, 3, respectively. To evaluate, i_{c1}, the secondary controller of source-1 evaluates the average of i_{s1}, i_{s2} and i_{s3}. However, due to the action of the link failure detection algorithm [31], [32], the secondary controllers of source-1 and source-2 evaluate the circulating currents, i_{c1} and i_{c2} using the average of source currents, (i_{s1}, i_{s3}) and (i_{s2}, i_{s3}), respectively. The waveforms of circulating current, source currents and source voltage under the link failure condition are shown in Fig. 14. The link failure occurs at the instant of t=1s. At time instant, t=1.5, the communication link is again restored between source-1 and 2. From the waveforms of i_{c1}, i_{c2} and i_{c3} shown in Fig. 14(a), it is observed that the proposed secondary controller ensures the convergence of circulating currents, i_{c1}, i_{c2} and i_{c3} to the tolerance limit, ε even in the case of one of the communication link failure. This validates the resiliency of the DC microgrid against the communication link failure. The waveforms of source currents, i_{s1}, i_{s2} and i_{s3} and the waveforms of source voltages v_{s1}, v_{s2} and v_{s3} are shown in Figs. 14(b) and 14(c).

4.6 Comparison of Performance of the proposed secondary controller with respect to the prior study

The performance of the proposed secondary controller is compared to the secondary controller suggested in [24], including the linear proportional plus integral controller to modify the droop gain of the source. The droop gain is modified by using the average of source currents. However, the secondary controller proposed in the revised manuscript includes an integral controller to shift the V-I droop characteristics of the source parallel to the voltage axis to minimize the circulating current. The proposed controller utilizes the proportional current rather than the average current to minimize the circulating current. The proportional current will be the same as the average current when all sources have identical ratings. However, in the case of sources having different ratings, proportional current has the advantage over average current. The same has been explained next.

For simplicity of understanding, a two-source system is considered. It is assumed that the sources have different ratings I_1 and I_2. Source-1 supplies a current $i_{1p.u}$ and source-2 supplies $i_{2p.u}$ concerning their bases. So, the total load demand of the system is $(i_{1p.u}I_1 + i_{2p.u}I_2)$.

When average per-unit current is used, the reference currents for both sources are $(\frac{i_{1pu}+i_{2pu}}{2})$, which in their bases become $(\frac{i_{1pu}+i_{2pu}}{2})I_1$ and $(\frac{i_{1pu}+i_{2pu}}{2})I_2$. Adding up these two current references, the total current commanded from both sources is $(\frac{I_1+I_2}{2})i_{1p.u} + (\frac{I_1+I_2}{2})i_{2p.u}$. However, the total load demand $(i_{1p.u}I_1 + i_{2p.u}I_2)$. The error between total load demand and total current commanded to both sources is $(i_{1p.u}\text{-}i_{2p.u})_{(\frac{I_1-I_2}{2})}$.

Therefore, average per-unit current can lead to excess/less supply of current by the sources. This will not lead to the flow of nonzero value of circulating current flowing

between the source converters. Consequently, the voltage regulation may become poor. This is a major shortcoming of using the average per-unit current-based secondary controller suggested in [24]. Now using (16), the current reference generated for source-1 is given by,

$$I_{1ref} = I_{d1} = \left(\frac{i_{1pu}I_1 + i_{2pu}I_2}{P_1\left(\frac{1}{P_1} + \frac{1}{P_2}\right)}\right) \tag{42}$$

Now using (12) for two sources, $P_1 d_1 = P_2 d_2 = k$. Therefore, $d_1 = k/P_1$ and $d_2 = k/P_2$. This helps us to simplify I_{1ref} as,

$$I_{1ref} = I_{d1} = \left(\frac{i_{1pu}I_1 + i_{2pu}I_2}{P_1 + P_2}\right)P_2 \tag{43}$$

Similarly, the expression for I_{2ref} is given by,

$$I_{2ref} = I_{d2} = \left(\frac{i_{1pu}I_1 + i_{2pu}I_2}{P_1 + P_2}\right)P_1 \tag{44}$$

The addition of references for the total proportional current is ($i_{1p.u}I_1 + i_{2p.u}I_2$). Thus, the total load demand is the same as the total current commanded to the sources.

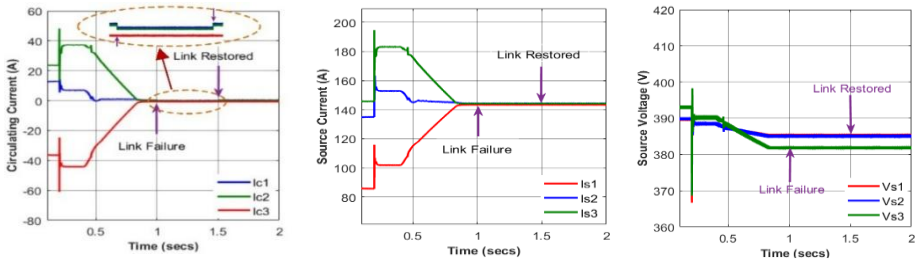

Figure 14. Waveforms of (a) Circulating currents, i_{c1}, i_{c2} and i_{c3} (b) Source currents, i_{s1}, i_{s2} and i_{s3}. (c) Source voltages, v_{s1}, v_{s2} and v_{s3} in case of link failure between source 2 and 3.

This is true irrespective of the ratings of the source and the per-unit currents being supplied by the source. Hence, using proportional current in place of average per-unit current for the system with different ratings will give better performance. This point can be further clarified by practical examples.

Consider 2 sources, one has ratings as 500 A and 500 V, and the other one is rated 250 A, 500 V. They are supposed to supply a load of 650 A. Initially, let the two source currents be 400 A and 250 A due to transmission line resistances. Using proportional current, the reference currents set for the two sources as 443.33 A and 216.67 A which matches the total current demand. However, using average per-unit current, the reference currents for the two sources are set as 450 A and 225 A. In this case, the total current reference then will be 675 A, which is more than the current demanded by the load.

Similarly, if these two sources are supplying 450 A and 200 A, average per-unit current sets references of source-1 and source-2 as 425 A and 212.5 A. Total current commanded is 637.5A which is less than the actual load demand. However, proportional current reference in this case is same as in the case above.

Also, as apparent from the above two examples, reference for per-unit average is dependent on the distribution of load currents which is not the case for proportional current. This is another drawback of per-unit average.

These two drawbacks make proposed proportional current based secondary controller more appealing to authors than per-unit average current based secondary controller suggested in [24].

4.7 Controller Hardware-In-Loop (CHIL) Results

In this subsection, the Controller Hardware-In-Loop (CHIL) based results are discussed. The CHIL setup includes the Real Time Digital Simulator (RTDS) and the Digital Signal Processor (DSP) of TI TMSF28379D as shown in Fig. 15. RSCAD is software which is used by the RTDS. The controllers are implemented in DSP.

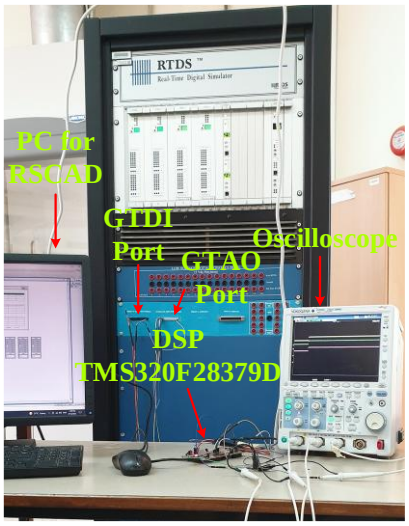

Figure 15. RTDS setup used to capture CHIL results of dc microgrid at Qatar University.

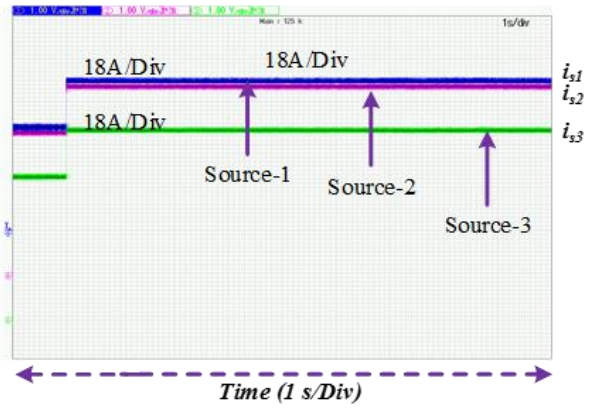

Figure 16: Controller hardware-in-loop (CHIL) results. Waveforms of currents supplied by dc-dc converters of source-1, source-2 and source-3.

The analogue signals generated by the simulated model of the DC Microgrid are supplied to the sensing board using a Giga Transceiver Analog Output (GTAO) card, which is mounted on the hardware module of RTDS. The DSP process these analogue signals and the digital output PWM pulses are generated by the controller implemented in DSP. These generated PWM pulses are supplied to various switches of dc-dc converters simulated in RTDS using a Giga-Transceiver Digital Input (GTDI) card.

DC Microgrid including three sources and three loads connected the ring configuration of interconnecting shown in Fig. 8 is simulated in RSCAD. The parameters of the DC Microgrid simulated in RTDS are the same as that of the parameters listed in Tables 2 and 3. Initially, the loads connected across the source bus-1, 2 and 3 are 25kW each. Fig. 16 shows the waveforms of currents supplied by source-1, source-2 and source-3. At time instant t=0.2s, the load at source bus-2 and source-3 is changed from 25kW to 35kW and 25kW to 40kW. From these waveforms, it is observed that as soon as the load demand is changed, the current immediately settles down at its steady state value within 20ms. This validates the fast dynamic response of the converters.

The nominal voltage of source-2 is 400 V. The error in the nominal value of source voltage-1 and 3 is -1% and 1% respectively, of the base nominal value of source voltages. Due to an error in the voltage sensors of source-1 and source-3, the nominal voltages of these sources are 396V and 404V, respectively. The Figs. 17(a) and 17(b) show the waveforms of the circulating currents flowing among the source-1, source-2 and source-3. At time instant t=0s, the DC microgrid operates under the action conventional droop controller. The circulating currents flowing among the sources are calculated using the relation (9). The circulating current flowing into source-1 is -11A while the circulating current supplied by source-2 and source-3 is 5.5A each. The

circulating current continues to flow among the sources. The error in current sharing for source-1, 2 and 3 are listed in Table 4 and are 4.4%, 2.2% and 2.2%, respectively. To minimize these circulating currents, the proposed secondary controller is switched on at a time instant of t =2s. Due to the action of the proposed controller, a positive shift, vshift1 takes place in the nominal voltage of source-1, while the negative shifts, vshift2 and vshift3 take place in the nominal voltages of source-2 and source-3 as shown in Figs. 18(a) and 18(b). The magnitude of vshift1 is 4.5V while the magnitudes of vshift2 and vshift3 are -3.0V and -3.5V, respectively. Due to these shifts in nominal voltages of the sources, the circulating current flowing into source-1 is minimized to 1 A while the value of circulating currents for source-2 and source-3 is 0.5A each which is shown in Figs. 17(a) and 17(b).

Fig. 19 shows the waveforms of currents supplied by source-1, source-2 and source-3. Before the time instant t=1s, the current supplied by source-1 is 70A while the currents supplied by source-2 and 3 are 87A each. At time instant, t=1s, the proposed secondary controller is switched on. Due to the action of the proposed controller, the redistribution of currents takes place among source-1, source-2 and source-3. At time instant, t=5s, the currents supplied by source-1, source-2 and source-3 are settled to 81A, 82A and 81.5A, respectively.

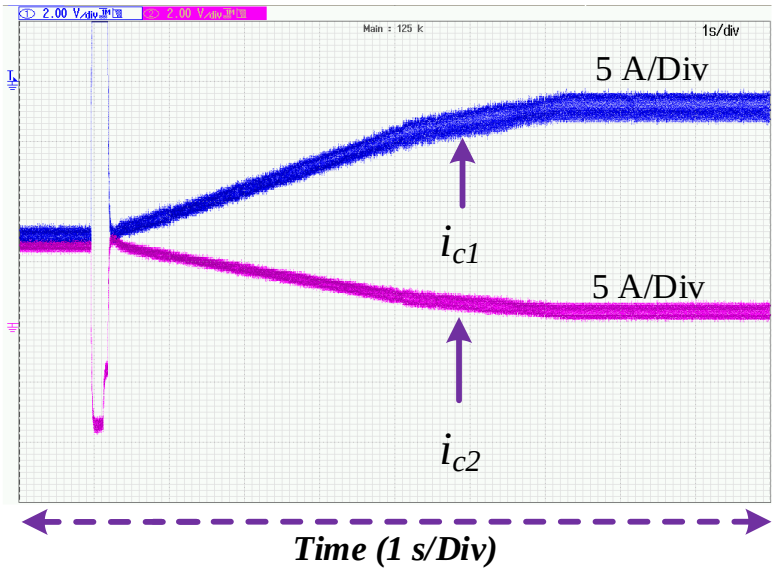

(a)

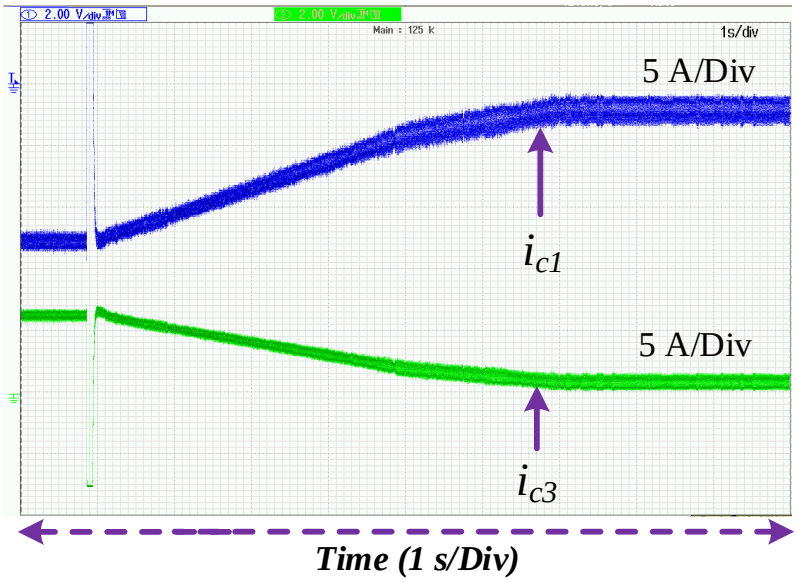

(b)

Figure 17: Controller hardware-in-loop (CHIL) results. Waveforms of circulating currents, ic1, ic2 and ic3 flowing among the source-1, source-2 and source-3. (Voltage shift: 5 A/div, time-axis: 1 s/div).

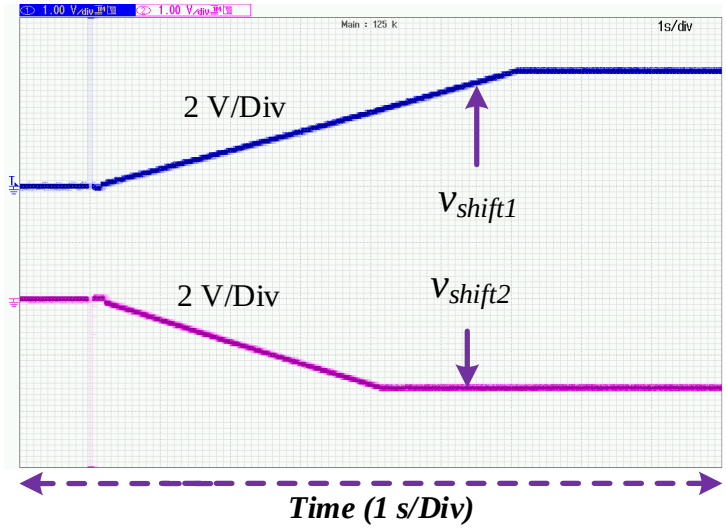

(a)

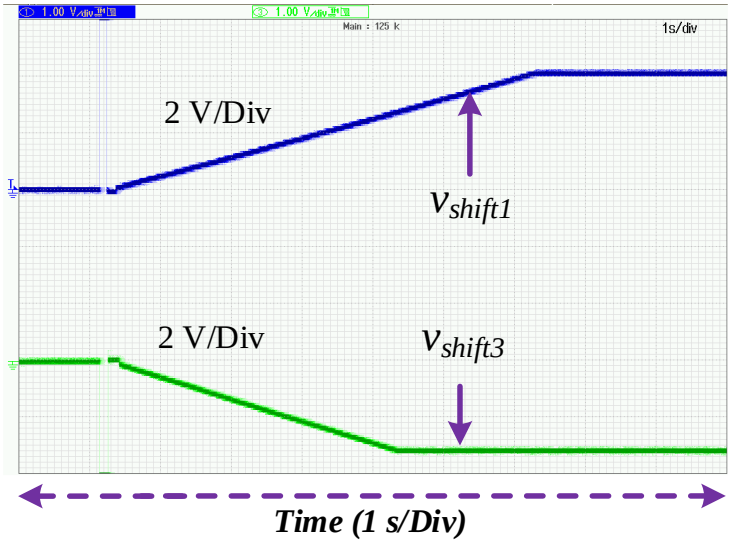

(b)

Figure 18. Controller hardware-in-loop (CHIL) results. Waveforms of voltage shifts, (a) vshift1, and vshift2 (b) vshift1 and vshift3 provided by the proposed secondary controller in the nominal voltages of source-1, 2 and 3.

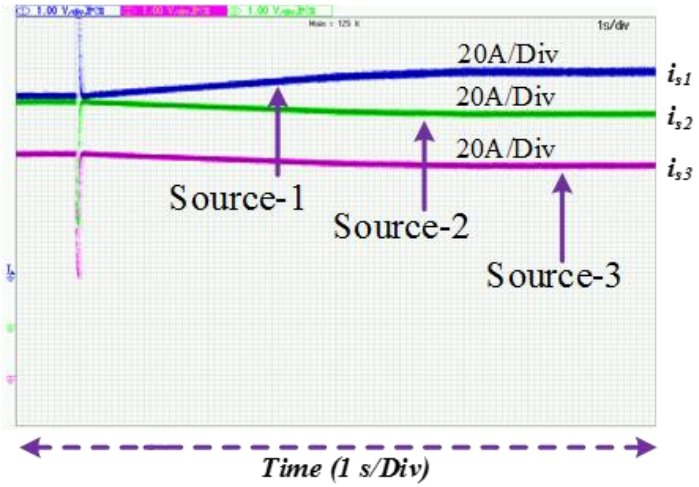

Figure 19. Controller hardware-in-loop (CHIL) results. Waveforms of currents supplied by source-1, source-2 and source-3.

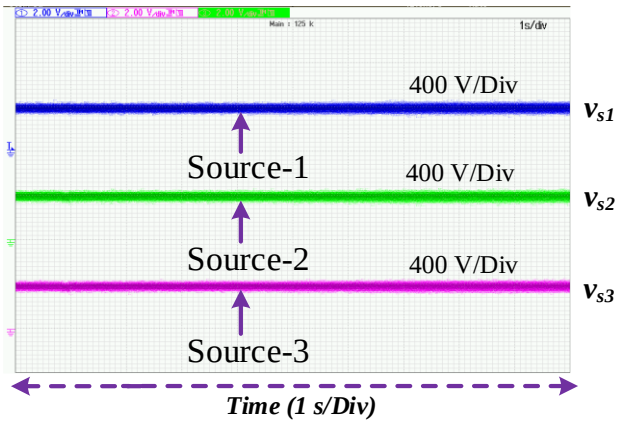

Figure 20. Controller hardware-in-loop (CHIL) results. Waveforms of voltages across the terminals of dc-dc boost converters of source-1, source-2 and source-3.

Fig. 20 shows the waveforms of source voltage-1, 2 and 3. Initially, the voltage across source-1, 2 and 3 are 392.2 V, 396.5 V and 400 V respectively. After the voltage shift in nominal voltages, the final values of source-1, 2 and 3 voltages are 396.4 V,

393.7 V and 396.5 V respectively. The voltage regulations appearing across the terminals of the dc-dc boost converter connected across the source-1, 2 and source-3 are listed in Table 4. Using conventional droop law, the voltage regulations across the converters are 2.25%, 1.75% and 1.6%. The proposed secondary controller is switched on at a time instant of t=2s. Due to the action of the proposed controller, a positive shift, vshift1 takes place in the nominal voltage of source-1, while the negative shifts, vshift2 and vshift3 take place in the nominal voltages of source-2 and source-3 The proposed secondary controller ensures voltage regulation across the converter ends of source-1, 2 and 3 as 2.5%, 2.25% and 2.12%.

From Table 4, the voltage regulation appearing across the terminals of source-1, 2 and 3 using the proposed secondary controller is observed to be less than 5%. This eliminates the need for a controller required to improve voltage regulation across the source converters. These waveforms validate the efficacy of the proposed controller used to minimize circulating currents flowing among the source converter due to unequal values of nominal voltages.

Table 4: Percentage of circulating current and voltage regulation using conventional droop control law and proposed secondary controller.

Source	Circulating Current (%)		Voltage regulation (%)	
	Conventional	Proposed	Conventional	Proposed
1	4.4%	0.4%	2.25	2.5
2	2.2%	0.2%	1.75	2.25
3	2.2%	0.2%	1.6	2.12

4.8 Summary

Chapter 4 presents a detailed evaluation of the proposed distributed secondary controller using simulations and Controller Hardware-In-Loop (CHIL) experiments to validate its performance under diverse conditions. A DC microgrid with three sources connected in a ring configuration was analyzed, considering scenarios with both equal and unequal power ratings among the sources. For the equal power case, three 100 kW sources were simulated, with errors of -1% and +1% introduced in the nominal voltages of source-1 and source-3, respectively, and a load demand of 50 kW on each source. When the load on buses 2 and 3 increased to 60 kW and 70 kW at t =2s, circulating currents reached -44 A, 7 A, and 37 A. The proposed controller, activated at t = 0.4s reduced these to within the tolerance limit of 0.5%, achieving an average source current of 147 A with voltage regulation between 2.5% and 3.25%, well below the 5% threshold. For unequal power ratings of 100 kW, 50 kW, and 25 kW, with corresponding droop gains of 0.076 Ω, 0.152 Ω, and 0.304 Ω, circulating currents due to an initial load of 25 kW on each bus reached -33 A, 10 A, and 23 A. After the controller was activated at t = 0.4s, these currents were reduced to within 0.5% tolerance, with source currents settling at 150A, 75A, and 37.5A, proportional to their ratings, while maintaining voltage regulation within 3.25%. The controller's resilience was tested under a communication link failure between source-1 and source-2 at t = 1.0s during which circulating currents remained within the acceptable tolerance due to the controller's adaptive mechanisms. When the link was restored at t =1.5s, normal operation resumed seamlessly, demonstrating the system's fail-safe behavior. CHIL experiments further validated the results, showing dynamic stability during load changes with circulating currents reduced to less than 1A and voltage shifts of +4.5 V, −3.0 V, and −3.5 V for sources 1, 2, and 3, respectively. Compared to traditional droop controllers and previous secondary control

methods, the proposed approach achieved faster response, improved proportional current sharing, and reduced voltage regulation errors from 4.4% to under 3.25%, highlighting its superior performance and robustness for modern DC microgrid challenges.

CHAPTER 5: CONCLUSION AND FUTURE WORK

5.1 Conclusion

The circulating current flowing among sources connected in a DC Microgrid is a serious concern. The circulating current flows due to unequal nominal voltages of the source converters. The unequal nominal voltages occur due to errors in the measurement of voltage sensors included in source converters. In a source converter, the voltage sensor supplies a feedback signal to the voltage controller. A nonzero value of circulating current may lead to losses, decrement in efficiency, draining of battery, and overloading of converters. This in turn may lead to premature failure of converters. To resolve this issue, a distributed secondary controller is suggested in this project. The proposed controller computes the circulating current flowing among the sources. If this current is greater than the tolerance value of the circulating current, the proposed controller keeps on shifting the droop characteristics of the source parallel to the voltage axis until the circulating current is minimized below the tolerance value. To shift droop characteristics, the proposed controller includes an integrator. To validate the efficacy of the proposed controller, results are captured using the CHIL setup. The error in proportional current sharing due to the conventional and proposed controller for source-1 is observed to be 4.4% and 0.4% respectively. The voltage regulation across the source converter using conventional droop control law and the proposed secondary controller for source-1 is 2.25% and 2.5%, respectively. This validates the effectiveness of the controller's performance. Root loci plots are used to study the impact of variation in the parameters of the proposed controller on the stability of the DC Microgrid. From this plot, it is observed that the stability margin of the DC Microgrid decreases with an increase in the gain of the proposed secondary controller. The proposed secondary maintain current sharing accuracy in case of microgrid having sources of unequal

capacity. Further, the proposed secondary ensures the fail-safe behaviour of the DC microgrid in case of communication link failure.

5.2 Future work

Building on the progress made in this research, there are several promising areas for future exploration that could improve the performance and flexibility of the proposed distributed secondary controller. These ideas aim to solve current challenges and expand its practical uses in the DC microgrid systems:

- Managing Renewable Energy Variability: Solar and wind energy sources can cause oscillations that affect grid stability. Future study should concentrate on developing predictive or adaptive algorithms to account for these changes, ensuring constant performance even during periods of unpredictability.
- Adapting to Changing Load Patterns: Although this study concentrated on static load circumstances, real-world scenarios may include dynamic and unanticipated load variations. Investigating how the controller operate with different kinds of loads, such as industrial equipment cycles or smart home demands.
- Improving Resilience to Communication Failures: Building on the system's fail-safe features, future work could explore advanced strategies to maintain stability and control even when communication links are interrupted. This would make the controller even more robust in real-world conditions.
- Scalability for Larger Microgrids: As microgrids increase in size and complexity, the proposed controller's ability to handle these larger systems must be examined.

5.3 Publications List

- This thesis has made a significant contribution to the field, resulting in the publication of the paper: S. Islam, A. Khalfalla, M. Hamoud, H. Mehrjerdi, A. Iqbal, and V. Marzang, 'Distributed Secondary Controller to Minimize Circulating Current Flowing Among Sources in DC Microgrid,' in *IEEE Access, vol. 11,* pp. 89488–89505, 2023, doi: 10.1109/ACCESS.2023.3305369."
- This thesis has provided a valuable contribution to the field, resulting in the acceptance of the paper: A. Khalfalla, S. Islam, and A. Iqbal, 'Distributed Secondary Controller to Minimize Circulating Current Flowing Among Sources in DC Microgrid,' in *11th IEEE International Conference on Power Electronics, Drives, and Energy Systems (PEDES) 2024.*
- This work was presented as a poster at the *4th QU Creativity & Innovation for Engineering Solutions Development Conference*. , which was held at Qatar University on April 21-22, 2024.

References

[1] Ko, B.S., Lee, G.Y., Choi, K.Y. and Kim, R.Y., 2018. A coordinated droop control method using a virtual voltage axis for power management and voltage restoration of DC microgrids. *IEEE Transactions on Industrial Electronics*, *66*(11), pp.9076-9085.

[2] Sharma, S., Iyer, V.M., Bhattacharya, S. and Zou, K., 2023. New mesh configurations with decentralized droop control method for DC microgrids. *IEEE Transactions on Industrial Electronics*, *71*(1), pp.560-571.

[3] Khosravi, N., Dowlatabadi, M. and Sabzevari, K., 2025. A hierarchical deep learning approach to optimizing voltage and frequency control in networked microgrid systems. *Applied Energy*, *377*, p.124313.

[4] Sevostyanov, N.A. and Gorbunov, R.L., 2023. Control strategy to mitigate voltage ripples in droop-controlled DC microgrids. *IEEE Transactions on Power Electronics*.

[5] Qi, L.L., Gao, M. and Faddel, S., 2024. Comparative Study of Four Droop Control Strategies in Buck Converter Based DC Microgrid. *IEEE Transactions on Industry Applications*.

[6] Carnaghi, M., Cervellini, P., Judewicz, M., Retegui, R.G. and Funes, M., 2023. Stability analysis of a Networking DC microgrid with distributed droop control and CPLs. *IEEE Latin America Transactions*, *21*(9), pp.966-975.

[7] Xu, Z., Chen, F., Chen, K. and Lu, Q., 2024. Research on Adaptive Droop Control Strategy for a Solar-Storage DC Microgrid. *Energies*, *17*(6), p.1454.

[8] Dadi, R., Meenakshy, K. and Damodaran, S.K., 2023. A review on secondary control methods in DC microgrid. *Journal of Operation and Automation in Power Engineering*, *11*(2), pp.105-112.

[9] Mesbah, M.A., Sayed, K., Ahmed, A., Aref, M., Elbarbary, Z.M.S., Almuflih, A.S. and Mossa, M.A., 2024. Adaptive control approach for accurate current sharing and voltage regulation in DC microgrid applications. *Energies*, *17*(2), p.284.

[10] Al-Ismail, F.S., 2024. A critical review on DC microgrids voltage control and power management. *IEEE Access*.

[11] Jain, D. and Saxena, D., 2023. Comprehensive review on control schemes and stability investigation of hybrid AC-DC microgrid. *Electric Power Systems Research*, *218*, p.109182.

[12] Taye, B.A. and Choudhury, N.B.D., 2023. A dynamic droop control for a DC microgrid to enhance voltage profile and proportional current sharing. Electric Power Systems Research, 221, p.109438.

[13] Poonahela, I., Krama, A., Bayhan, S., Fesli, U., Shadmand, M.B., Abu-Rub, H. and Begovic, M.M., 2023. Hierarchical model-predictive droop control for voltage and frequency restoration in AC microgrids. *IEEE Open Journal of the Industrial Electronics Society*, *4*, pp.85-97.

[14] Liu, S., Miao, H., Li, J. and Yang, L., 2023. Voltage control and power sharing in DC Microgrids based on voltage-shifting and droop slope-adjusting strategy. *Electric Power Systems Research*, *214*, p.108814.

[15] Yang, C., Gao, F. and Zhang, B., 2024. An improved nonlinear droop control strategy in DC microgrids. *IEEE Transactions on Power Electronics*.

[16] Hassan, M.A., Su, C.L., Pou, J., Sulligoi, G., Almakhles, D., Bosich, D. and Guerrero, J.M., 2022. DC shipboard microgrids with constant power loads: A review of advanced nonlinear control strategies and stabilization techniques. *IEEE Transactions on Smart Grid*, *13*(5), pp.3422-3438.

[17] Kumar, R. and Pathak, M.K., 2020. Distributed droop control of dc microgrid for improved voltage regulation and current sharing. *IET Renewable Power Generation*, *14*(13), pp.2499-2506.

[18] Strasser, T., Andren, F., Kathan, J., Cecati, C., Buccella, C., Siano, P., Leitao, P., Zhabelova, G., Vyatkin, V., Vrba, P. and Mařík, V., 2014. A review of architectures and concepts for intelligence in future electric energy systems. *IEEE Transactions on Industrial Electronics*, *62*(4), pp.2424-2438.

[19] Lotfi, H. and Khodaei, A., 2015. AC versus DC microgrid planning. *IEEE Transactions on Smart Grid*, *8*(1), pp.296-304.

[20] Gu, Y., Li, W. and He, X., 2015. Analysis and control of bipolar LVDC grid with DC symmetrical component method. *IEEE transactions on power systems*, *31*(1), pp.685-694.

[21] Choi, B., 1998. Comparative study on paralleling schemes of converter modules for distributed power applications. *IEEE Transactions on industrial electronics*, *45*(2), pp.194-199.

[22] Morstyn, T., Hredzak, B., Demetriades, G.D. and Agelidis, V.G., 2015. Unified distributed control for DC microgrid operating modes. *IEEE Transactions on Power Systems*, *31*(1), pp.802-812.

[23] Moayedi, S. and Davoudi, A., 2015. Distributed tertiary control of DC microgrid clusters. *IEEE Transactions on Power Electronics*, *31*(2), pp.1717-1733.

[24] Lai, J., Lu, X., Yu, X., Yao, W., Wen, J. and Cheng, S., 2018. Distributed multi-DER cooperative control for master-slave-organized microgrid networks with limited communication bandwidth. *IEEE Transactions on Industrial Informatics*, *15*(6), pp.3443-3456.

[25] Federico, I., Jose, E. and Luis, F., 2017. Master–slave DC droop control for paralleling auxiliary DC/DC converters in electric bus applications. *IET Power Electronics*, *10*(10), pp.1156-1164.

[26] Garcerá, G., Figueres, E., Pascual, M. and Benavent, J.M., 2004. Robust model following control of parallel buck converters. *IEEE Transactions on Aerospace and Electronic Systems*, *40*(3), pp.983-997.

[27] Lai, Y.M., Tan, S.C. and Tsang, Y.M., 2009. Wireless control of load current sharing information for parallel-connected DC/DC power converters. *IET Power Electronics*, *2*(1), pp.14-21.

[28] Anand, S. and Fernandes, B.G., 2012. Modified droop controller for paralleling of dc–dc converters in standalone dc system. *IET Power Electronics*, *5*(6), pp.782-789.

[29] Guerrero, J.M., Vasquez, J.C., Matas, J., De Vicuña, L.G. and Castilla, M., 2010. Hierarchical control of droop-controlled AC and DC microgrids—A general approach toward standardization. *IEEE Transactions on industrial electronics*, *58*(1), pp.158-172.

[30] Augustine, S., Mishra, M.K. and Lakshminarasamma, N., 2014. Adaptive droop control strategy for load sharing and circulating current minimization in low-voltage standalone DC microgrid. *IEEE Transactions on Sustainable Energy*, *6*(1), pp.132-141.

[31] Li, Y., Jones, E.A. and Wang, F., 2016. Circulating current suppressing control's impact on arm inductance selection for modular multilevel converter. *IEEE Journal of Emerging and Selected Topics in Power Electronics*, *5*(1), pp.182-188.

[32] Yang, L., Chen, Y., Luo, A., Wu, W., Huai, K., Zhou, X., Zhou, L., Xu, Q. and Guerrero, J.M., 2016. Second ripple current suppression by two bandpass filters and current sharing method for energy storage converters in DC microgrid. *IEEE Journal of Emerging and Selected Topics in Power Electronics*, *5*(3), pp.1031-1044.

[33] A. Nawaz, J. Wu, and C. Long, "Mitigation of circulating currents for proportional current sharing and voltage stability of isolated DC microgrid," *Electr. Power Syst. Res.*, vol. 180, p. 106123, Mar. 2020, doi: 10.1016/j.epsr.2019.106123.